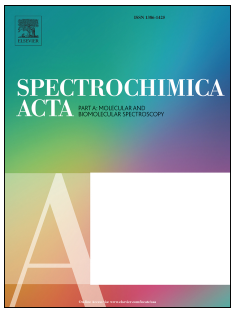

New ruthenium polypyridyl complexes functionalized with fluorine atom or furan: Synthesis, DNA-binding, cytotoxicity and antitumor mechanism studies

Guang-Bin Jiang, Wen-Yao Zhang, Miao He, Yi-Ying Gu, Lan Bai, Yang-Jie Wang, Qiao-Yan Yi, Fan Du

PII: S1386-1425(19)30924-2

DOI: https://doi.org/10.1016/j.saa.2019.117534

Reference: SAA 117534

To appear in: *Spectrochimica Acta Part A: Molecular and Biomolecular Spectroscopy*

Received Date: 24 July 2019

Revised Date: 27 August 2019

Accepted Date: 13 September 2019

Please cite this article as: G.-B. Jiang, W.-Y. Zhang, M. He, Y.-Y. Gu, L. Bai, Y.-J. Wang, Q.-Y. Yi, F. Du, New ruthenium polypyridyl complexes functionalized with fluorine atom or furan: Synthesis, DNA-binding, cytotoxicity and antitumor mechanism studies, *Spectrochimica Acta Part A: Molecular and Biomolecular Spectroscopy* (2019), doi: https://doi.org/10.1016/j.saa.2019.117534.

DNA-binding behaviors of the Ru(II) complexes were studied. Antitumor activity of Ru(II) complexes were assessed by MTT method. Moreover, the antitumor activity in vitro, morphological changes, mitochondrial membrane potentials, ROS levels, cellular localization, cell invasion, apoptosis, and cell cycle arrest were investigated.

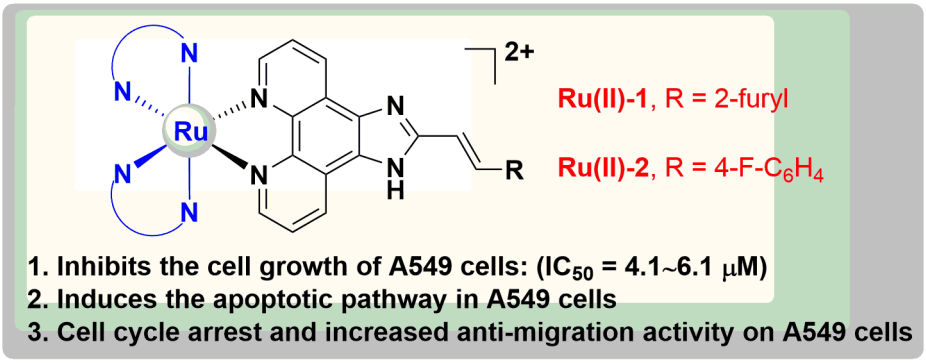

Submitted to Spectrochimica Acta Part A: Molecular and Biomolecular Spectroscopy

New Ruthenium Polypyridyl Complexes Functionalized with Fluorine Atom or Furan: Synthesis, DNA-binding, Cytotoxicity and Antitumor Mechanism Studies

Guang-Bin Jiang,[a,*] Wen-Yao Zhang,[b] Miao He,[b] Yi-Ying Gu,[b] Lan Bai,[b] Yang-Jie Wang,[b] Qiao-Yan Yi,[b] Fan Du[b]

[a]*Guangxi Key Laboratory of Electrochemical and Magnetochemical Function Materials, College of Chemistry and Bioengineering, Guilin University of Technology, Guilin, 541004, China.*

[b]*School of Pharmacy, Guangdong Pharmaceutical University, Guangzhou, 510006, PR China*

* Corresponding authors. Tel: +86-773-899-1304; fax: +86-773-899-1304.

E-mail address: jianggb@glut.edu.cn (G.B. Jiang).

Abstract Two novel ruthenium(II) polypyridyl complexes, namely, $[Ru(dmp)_2(CAPIP)](ClO_4)_2$ (**Ru(II)-1**) and $[Ru(dmp)_2(CFPIP)](ClO_4)_2$ (**Ru(II)-2**), which respectively contain (*E*)-2-(2-(furan-2-yl)vinyl)-1*H*-imidazo[4,5-*f*][1,10]phenanthroline (CAPIP) and (*E*)-2-(4-fluorostyryl)-1*H*-imidazo[4,5-*f*][1,10]phenanthroline (CFPIP), were first designed and characterized (dmp = 2,9-dimethyl-1,10-phenanthroline). DNA binding experiments indicated that Ru(II) complexes interact with CT DNA through intercalative mode. In addition, the complexes **Ru(II)-1** and **Ru(II)-2**, showed remarkable cell cytotoxicity, giving the respective IC_{50} values of 4.1 ± 1.4 μM and 6.1 ± 1.4 μM on the A549 cancer cells. These values indicated higher activity than CAPIP, CFPIP, cisplatin (8.2 ± 1.4 μM) and other corresponding Ru(II) polypyridyl complexes. Furthermore, the Ru(II) complexes could arrive the cytoplasm through the cell membrane and accumulate in the mitochondria. Significantly, complexes **Ru(II)-1** and **Ru(II)-2** induced A549 cells apoptosis was mediated by increase of ROS levels and dysfunction of mitochondria, and resulted in cell cycle arrest and increased anti-migration activity on A549 cells. Overall, these results indicated that complexes **Ru(II)-1** and **Ru(II)-2** could be suitable candidates for further investigation as a chemotherapeutic agent in the treatment of tumors.

Keywords: Ru(II) polypyridyl complex; DNA binding; antitumor; reactive oxygen species; cell cycle arrest.

1. Introduction

Although chemotherapy with platinum complexes is still one of the most frequently-used treatments for malignant tumors, its clinical application is limited by systemic toxicities, nervous system damage, and drug resistance [1-9]. Therefore, the search for alternative metal-based complexes with potential antitumor activities has evoked extensive investigations [10-17]. Ruthenium-containing complexes have been paid more attentions in recent years and considered as one of the most likely alternatives to platinum-based antitumor drug, because most of them have favorable properties, such as rich synthetic chemistry, low toxicity to normal cells and high antitumor activity [18-28]. Currently, ruthenium complexes NAMI-A and KP1019 have successfully reached the II-phase of clinical trials and have effectively convinced the pharmacologists to detect ruthenium-based antitumor agents [29]. Liu et al. described three ruthenium(II) polypyridyl complexes ($[Ru(N\text{-}N)_2(MHPIP)](ClO_4)_2$) that exerted excellent cytotoxic activity toward HepG-2 cells through DNA damage and mitochondria-mediated apoptosis induction pathway [30]. In 2014, Liang found that HSA-$[RuCl_5(ind)]^{2-}$ complex induces MGC-803 cells apoptosis, additionally, the Ru(II) complexes also inhibit the cell growth in MGC-803 cells at G2 phase.[31] Very recently, our group reported that complexes $[Ru(N\text{-}N)_2(BTPIP)](ClO_4)_2$ could induce apoptosis in A549 cells via a mitochondrial dysfunction pathway [32].

Heterocycles and fluorine atom are significant structural fragments which have attracted widespread attention from the pharmaceutical industry since they can be used to modify different types of drug molecules, impacting their solubility and

lipophilicity, and altering their pharmacokinetic and pharmacodynamics properties [33-36]. Nonetheless, fluorine-containing and furan-based Ru(II) polypyridyl complexes are rarely detected as antitumor drugs, As part of our continuous and deep studies on the antitumor activity of Ru(II) complexes, herein, we designed and synthesized two novel ruthenium complexes containing furan group and fluorine atom: $[Ru(dmp)_2(CAPIP)](ClO_4)_2$ (**Ru(II)-1**) and $[Ru(dmp)_2(CFPIP)](ClO_4)_2$ (**Ru(II)-2**). The Ru(II) complexes were characterized by HRMS, IR, NMR, etc. The antitumor activity in vitro, morphological changes, mitochondrial membrane potentials, ROS levels, cellular localization, cell invasion, apoptosis, and cell cycle arrest were investigated. In addition, DNA binding experiments were also explored. This research may be useful for the future development of Ru(II) polypyridyl complexes as potential chemotherapeutic agents.

2. Experimental section

2.1. Materials and methods

All reagents and solvents were purchased commercially and used without further purification unless otherwise noted. Calf thymus DNA (CT DNA) was obtained from the Sino American Biotechnology Company. Ltd. Ultrapure MilliQ water was used in all experiments. DMSO and RPMI 1640 were purchased from Sigma. Cell lines of HeLa (Human cervical cancer cell line), SGC-7901 (human gastric carcinoma cells), HepG-2 (Hepatocellular carcinoma cells) and A549 (Human lung carcinoma cells) were purchased from the American Type Culture Collection. $RuCl_3 \cdot 3H_2O$ was obtained from the Kunming Institution of Precious Metals.

2,9-Dimethyl-1,10-phenanthroline was obtained from the Guangzhou Chemical Reagent Factory.

Analytical thin layer chromatography was performed by using commercially prepared 100-400 mesh silica gel plates (GF_{254}) and visualization was effected at 254 nm. Mass spectra were recorded on a Thermo Scientific ISQ gas chromatograph-mass spectrometer. The data of HRMS was carried out on a high-resolution mass spectrometer (LCMS-IT-TOF). IR spectra were obtained either as potassium bromide pellets or as liquid films between two potassium bromide pellets with a Bruker TENSOR 27 spectrometer. ^{1}H NMR spectra were recorded on a Varian-500 spectrometer with DMSO-d_6 as solvent and tetramethylsilane (TMS) as an internal standard at 400 MHz at room temperature.

2.2. Synthesis of ligand and complexes

2.2.1. Synthesis of 1,10-phenanthroline-5,6-dione

Following a modified procedure [37], an ice cold mixture of concentrated H_2SO_4 (40 mL) and HNO_3 (20 mL) was added to 4.0 g of 1,10-phenanthroline and 4.0 g of KBr. After heated at 83 ^{o}C for 3 h, the hot yellow solution was poured over 500 mL of ice and neutralized carefully with strong caustic until neutral to slightly acidic pH. Next, extraction with $CHCl_3$ followed by drying with anhydrous $MgSO_4$, and then concentrated in vacuo. The resulting residue was further purified by recrystallization with ethanol to give the desired 1,10-phenanthroline-5,6-dione.

2.2.2. Synthesis of ligand (CAPIP)

A mixture of 1,10-phenanthroline-5,6-dione (210.0 mg, 1.0 mmol), (*E*)-3-(furan-2-yl)acrylaldehyde (122.0 mg, 1.0 mmol), ammonium acetate (30 mmol, 2312.4 mg) and acetic acid (45 mL) was refluxed with stirring for 4 h. The cooled solution was diluted with water and neutralized with concentrated aqueous ammonia (25 wt.%). The brown precipitate was collected and purified by column chromatography on silica gel (60~100 mesh) with ethanol as eluent to give the compound as a brown yellow powder. Yield: 271.4 mg, 87%. Anal. Calc for $C_{19}H_{12}N_4O$: C, 73.05%, H, 3.87%, N, 17.95%. Found: C, 73..12%, H, 3.82%, N, 17.88%; IR: ν = 3109, 1636, 1558, 1504, 1465, 1425, 1340, 1357, 1260, 1186, 1141, 1075, 1017, 804, 734, 657 cm^{-1}; ^1H NMR (400 MHz, DMSO-d_6) δ 9.01 (s, 2H， a, a′), 8.77 (d, J = 52.7 Hz, 2H, c, c′), 7.82 (s, 3H, b, b′, h), 7.57 (d, J = 16.2 Hz, 1H, d), 7.05 (d, J = 16.2 Hz, 1H, e), 6.83 (s, 1H, f), 6.64 (s, 1H, g); HRMS (ESI) m/z: calcd for $C_{19}H_{13}N_4O$ $[M+H]^+$, 313.1084; found 313.1081.

2.2.3. Synthesis of ligand (CFPIP)

A mixture of 1,10-phenanthroline-5,6-dione (210.0 mg, 1.0 mmol), (*E*)-3-(4-fluorophenyl)acrylaldehyde (150.0 mg, 1.0 mmol), ammonium acetate (30 mmol, 2312.4 mg) and acetic acid (45 mL) was refluxed with stirring for 4 h. The cooled solution was diluted with water and neutralized with concentrated aqueous ammonia (25 wt.%). The brown precipitate was collected and purified by column chromatography on silica gel (60~100 mesh) with ethanol as eluent to give the compound as a brown yellow powder. Yield: 278.8 mg, 82%. Anal. Calc for $C_{21}H_{13}FN_4$: C, 74.09%, H, 3.85%, N, 16.47%. Found: C, 74.01%, H, 3.89%, N,

16.52%; IR: ν = 3178, 1647, 1601, 1552, 1507, 1402, 1358, 1290, 1228, 1157, 1128, 1021, 863, 809, 740, 521 cm^{-1}; ^1H NMR (400 MHz, DMSO-d_6) δ 9.04 (d, J = 3.8 Hz, 2H, a, a′), 8.87 (d, J = 8.0 Hz, 2H, c, c′), 7.87-7.75 (m, 5H, b, b′, f, f′, g), 7.32 (dd, J = 21.3, 12.5 Hz, 3H, g′, j, k); HRMS (ESI) m/z: calcd for $C_{21}H_{14}FN_4$ $[M+H]^+$, 341.1197; found 341.1194.

*2.2.4. Synthesis of $[Ru(dmp)_2(CAPIP)](ClO_4)_2$ (**Ru(II)-1**)*

A mixture of *cis*-$[Ru(dmp)_2Cl_2]\cdot 2H_2O$ (189.9 mg, 0.3 mmol) and CAPIP (93.9 mg, 0.3 mmol) in ethylene glycol (12 mL) was heated at 150 ^oC under argon for 8 h to give a clear red solution. Upon cooling, a red precipitate was obtained by dropwise addition of saturated aqueous $NaClO_4$ solution. The crude product was purified by column chromatography on neutral alumina with a mixture of CH_3CN-toluene (3:2, v/v) as eluent. The red band was collected. The solvent was removed under reduced pressure and a red-brown powder was obtained. Yield: 207.0 mg, 69%. Anal. Calc for $C_{47}H_{36}Cl_2N_8O_9Ru$: C, 54.86%, H, 3.53%, N, 10.90%. Found: C, 54.98%, H, 3.57%, N, 10.83%; IR: ν = 3065, 1969, 1627, 1570, 1506, 1443, 1304, 1217, 1198, 961, 928, 856, 809, 729, 623, 556 cm^{-1}; ^1H NMR (400 MHz, DMSO-d_6) δ 8.94 (d, J = 8.3 Hz, 2H, a, a′), 8.79-8.70 (m, 2H, c, c′), 8.46 (t, J = 8.9 Hz, 4H, 2, 2′, 5, 5′), 8.27 (d, J = 8.7 Hz, 2H, 3, 3′), 8.00 (d, J = 8.3 Hz, 2H, 4, 4′), 7.80 (d, J = 10.8 Hz, 1H, h), 7.60 (dd, J = 16.3, 8.7 Hz, 1H, d), 7.43 (m, J = 22.6, 13.7, 5.0 Hz, 6H, b, b′, 1, 1′, 6, 6′), 6.96 (dd, J = 28.0, 16.3 Hz, 1H, e), 6.85 (d, J = 6.5 Hz, 1H, f), 6.64 (s, 1H, g), 1.97 (s, 6H, 7, 7′), 1.75 (d, J = 5.5 Hz, 6H, 8, 8′); ^{13}C NMR (100 MHz, DMSO-d_6) δ 168.4, 166.8, 153.1, 153.1, 151.9, 150.9, 149.4, 148.3, 146.0, 145.0, 144.9, 138.6, 137.2, 131.0, 130.0,

128.0, 127.9, 127.6, 127.0, 125.5, 123.2, 122.5, 115.0, 113.1, 112.9, 26.0, 25.0; HRMS (ESI) m/z: calcd for $C_{47}H_{35}N_8O_1Ru$ $[M\text{-}2ClO_4\text{-}H]^+$, 829.1984; found 829.1990.

*2.2.5. Synthesis of $[Ru(dmp)_2(CFPIP)](ClO_4)_2$ (**Ru(II)-2**)*

This complex was synthesized in an identical manner to that described for complex **Ru(II)-1**, with CFPIP [38,39] in place of CAPIP. Yield: 241.2 mg, 76%. Anal. Calc for $C_{49}H_{37}Cl_2FN_8O_8Ru$: C, 55.68%, H, 3.53%, N, 10.61%. Found: C, 55.57%, H, 3.60%, N, 10.69%; IR: ν = 3066, 1626, 1589, 1508, 1444, 1350, 1222, 1198, 1159, 1090, 972, 857, 828, 806, 623, 556 cm^{-1}; ^1H NMR (400 MHz, DMSO) δ 8.91 (d, *J* = 8.2 Hz, 2H, a, a′), 8.72 (d, J = 8.1 Hz, 2H, c, c′), 8.43 (t, *J* = 8.9 Hz, 4H, 2, 2′, 5, 5′), 8.24 (d, *J* = 8.7 Hz, 2H, 3,3′), 7.98 (d, *J* = 8.2 Hz, 2H,4, 4′), 7.66 (dd, *J* = 18.6, 11.6 Hz, 3H, b, b′, f), 7.38 (d, *J* = 7.9 Hz, 4H, f′, 6, 6′), 7.23 (dd, *J* = 20.6, 14.4 Hz, 5H, 1, 1′, g, g′, j, k), 1.96 (s, 6H, 7, 7′), 1.74 (s, 6H, 8, 8′); ^{13}C NMR (100 MHz, DMSO-d_6) δ 167.5 (d, *J* = 160.3 Hz), 163.6, 161.1, 157.5 (q, *J* = 2.0 Hz), 149.5, 149.4, 148.4, 145.3, 138.4, 137.1, 135.8 (d, *J* = 2.4 Hz), 133.6 (d, *J* = 2.6 Hz), 130.8, 130.7, 129.9 (d, *J* = 2.4 Hz), 129.1 (d, *J* = 7.5 Hz), 128.0, 127.8, 127.6, 126.9, 124.8, 124.4, 121.3, 116.3, 116.1, 25.9, 25.0; HRMS (ESI) m/z: calcd for $C_{49}H_{36}FN_8Ru$ $[M\text{-}2ClO_4\text{-}H]^+$, 857.2098; found 857.2101.

Caution: Perchlorate salts of metal compounds with organic ligands are potentially explosive, and only small amounts of the material should be prepared and handled with great care.

2.3. Ruthenium(II) complexes-CT-DNA binding

The DNA-binding experiments were performed at room temperature. Buffer A [5 mM Tris-HCl, 50 mM NaCl, pH 7.0] was used for absorption titration, and viscosity measurements. Buffer B (50 mM Tris-HCl, 18 mM NaCl, pH 7.2) was used for DNA photocleavage experiments. Solutions of CT DNA in buffer A gave a ratio of UV-Vis absorbance of 1.8~1.9:1 at 260 and 280 nm, indicating that the DNA was sufficiently free of protein [40]. The concentration of DNA was determined spectrophotometrically (ε_{260} = 6600 M^{-1} cm^{-3}) [41].

The absorption titrations of the complex in buffer were performed using a fixed concentration (5.0 μM) for complex to which increments of the DNA stock solution were added. The intrinsic binding constant *K*, based on the absorption titration, was measured by monitoring the changes in absorption at the MLCT (metal-to-ligand charge transfer) band with increasing concentration of DNA using the following equation [42].

$$[DNA]/(\varepsilon_a - \varepsilon_f) = [DNA]/(\varepsilon_b - \varepsilon_f) + 1/[K_b((\varepsilon_b - \varepsilon_f)] \quad (1)$$

Where [DNA] is the concentration of DNA in base pairs, ε_a, ε_f and ε_b correspond to the apparent absorption coefficient A_{obsd}/[Ru], the extinction coefficient for the free ruthenium complex and the extinction coefficient for the ruthenium complex in the fully bound form, respectively. In plots of [DNA]/(ε_a-ε_f) versus [DNA], K_b is given by the ratio of slope to the intercept.

Viscosity measurements were carried out using an Ubbelodhe viscometer maintained at a constant temperature at 25.0 (± 0.1) °C in a thermostatic bath. DNA

samples approximately 200 base pairs in average length were prepared by sonication to minimize complexities arising from DNA flexibility [43]. Flow time was measured with a digital stopwatch, and each sample was measured three times, and an average flow time was calculated. Relative viscosities for DNA in the presence and absence of complex were calculated from the relation $\eta = (t - t^0)/t^0$, where t is the observed flow time of the DNA-containing solution and t^0 is the flow time of buffer alone [44,45]. The change in the viscosity was presented as $(\eta/\eta_0)^{1/3}$ versus binding ratio [Ru]/[DNA] [46], where η is the viscosity of DNA solution in the presence of complexes and η_0 is the viscosity of DNA solution alone.

2.4. Cytotoxicity assay in vitro

Standard 3-(4,5-dimethylthiazole)-2,5-diphenyltetraazolium bromide (MTT) assay procedures were used [47,48]. Cells were placed in 96-well microassay culture plates (8×10^3 cells per well) and grown overnight at 37 °C in a 5% CO_2 incubator. The tested compounds were then added to the wells to achieve final concentrations ranging from 10^{-6} to 10^{-4} M. Control wells were prepared by addition of culture medium (100 μL). The plates were incubated at 37 °C in a 5% CO_2 incubator for 48 h. Upon completion of the incubation, stock MTT dye solution (20 μL, 5 mg·mL^{-1}) was added to each well. After 4 h, DMSO (100 μL) was added to solubilize the MTT formazan. The optical density of each well was then measured with a microplate spectrophotometer at a wavelength of 490 nm. The IC_{50} values were calculated by plotting the percentage viability versus concentration on a logarithmic graph and

reading off the concentration at which 50% of cells remained viable relative to the control. Each experiment was repeated at least three times to obtain the mean values.

2.5. Apoptosis assessment by AO/EB staining

A549 cells were seeded onto chamber slides in six-well plates at a density of 2 × 10^5 cells per well and incubated for 24 h. The cells were cultured in RPMI 1640 containing 10% of FBS and incubated at 37 ^oC in 5% CO_2. The medium was removed and replaced with medium (final DMSO concentration, 0.05% v/v) containing the complexes for 24 h. The medium was removed again, and the cells were washed with ice-cold phosphate buffer saline (PBS), and fixed with formalin (4%, w/v). Cell nuclei were counterstained with acridine orange (AO) and ethidium bromide (EB) (AO: 100 µg mL^{-1}, EB: 100 µgmL^{-1}) for 10 min. The cells were observed and imaged with a fluorescence microscope (Nikon, Yokohama, Japan) with excitation at 350 nm and emission at 460 nm.

2.6. Reactive oxygen species (ROS) levels studies

The levels of the ROS in A549 cells induced by the complexes were measured using the fluorescent dye 2′,7′-dichlorodihydrofluorescein diacetate (DCFH-DA). The cells were seeded in a 12-well plate with 2 × 10^5 cells each well, and incubated overnight. After being treated with different concentration of the complexes for 24 h, the cells were washed twice with cold PBS and subsequently prestained with DCFH-DA (10 mM) and incubated at 37 ^oC in the dark for 30 min. Afterward, the

treated cells were washed two times with cold PBS, and stained with Hoechest 33342 for 20 min in the dark at 37 ^{o}C. Finally, the cells were washed twice with PBS, and then imaged and quantitatively analyzed using a confocal fluorescence microscope.

2.7. The change of mitochondrial membrane potential assay

A549 cells were inoculated at a density of 2 × 10^5 cells/well in 12-well plates and incubated with or without different concentration of the complexes for 24 h at 37 ^{o}C, and then washed two times with PBS. Afterward, JC-1 dye (1 μg/mL) was added and incubated for 20 min in the dark at 37 ^{o}C. After being washed with PBS, the cells were suspended in PBS, and observed under an ImageXpress Micro XLS system.

2.8. Location assay of the complex in the mitochondria

A549 cells were placed in 12-well microassay culture plates (4 × 10^4 cells per well) and grown overnight at 37 ^{o}C in a 5% CO_2 incubator. 1.0 μM of the complexes were added to the wells at 37 ^{o}C in a 5% CO_2 incubator for 4 h and further co-incubated with MitoTracker® Deep Green FM (150 nM) at 37 ^{o}C for 0.5 h. Upon completion of the incubation, the wells were washed three times with ice-cold PBS. After discarding the culture medium, the cells were imaged under a fluorescence microscope.

2.9. Matrigel invasion assay

BD Matrigel invasion chamber was used to investigate cell invasion according to the manufacturer's instructions. A549 cells (4 × 10^4) in serum free medium

containing different concentrations of the complexes were seeded into the top chamber of the two-chamber Matrigel system. RPMI 1640 medium (20% FBS) was added into the lower chamber. The cells were allowed to invade for 24 h. After incubation, non-invading cells were removed from the upper surface and cells on the lower surface were fixed with 4% paraformaldehyde and stained with 0.1% crystal violet. The membranes were photographed and the invading cells were counted under a light microscope. The mean values from three independent assays were calculated.

3. Results and discussion

3.1 Synthesis and characterization

The ligands (*E*)-2-(2-(furan-2-yl)vinyl)-1*H*-imidazo[4,5-*f*][1,10]phenanthroline (CAPIP), (*E*)-2-(4-fluorostyryl)-1*H*-imidazo[4,5-*f*][1,10]phenanthroline (CFPIP) and corresponding Ru(II) complexes were prepared according to previously reported procedures, as illustrated in the experimental section. The crude Ru(II) complexes were purified by column chromatography on neutral alumina. In addition, the target complexes were characterized by NMR spectra, HRMS, IR and elemental analysis. In the IR spectra, the peaks of 1627 cm^{-1} for **Ru(II)-1** and 1626 cm^{-1} for **Ru(II)-2** are assigned the C=C stretching vibration. In the HRMS spectra for the complexes, all of the expected signals $[M\text{-}2ClO_4\text{-}H]^+$ and $[M\text{-}2ClO_4\text{-}H]^{2+}$ were detected. In the double bond of the ligands, the chemical shifts of 7.6 and 7.1 ppm are attributed to d and e, and 7.4 and 7.3 ppm are assigned to hydrogen atoms j and k. When the ligands bonded to metal to form Ru(II) complexes, the chemical shifts of the alkenyl

hydrogen in the complexes shown a weak red shift. The UV-Vis of Ru(II) complexes (5 μM) in PBS is shown in Fig. S2 (Supporting Information), the maximum absorbance of Ru(II) complexes appears at 467 nm (**Ru(II)-1**) and 469 nm (**Ru(II)-2**).

3.2. Cytotoxicity in vitro assays

We investigated the cytotoxicity of complexes **Ru(II)-1** and **Ru(II)-2** at various concentrations toward four human cancer cell lines (A549, HepG-2, SGC-7901, Hela). The half maximal inhibitory concentration values was detected by MTT method after exposure with ligand and Ru(II) complexes for 24 h, and the values are summarized in Table 1. As a result, ruthenium(II) complexes were found to be more active than CAPIP and CFPIP. Based on these findings, it can be concluded that the introduction of ruthenium is importance for anti-proliferative activity. It is worth noting that complexes **Ru(II)-1** (IC_{50} = 4.1 ± 1.4 μM) and **Ru(II)-2** (IC_{50} = 6.1 ± 1.6 μM) showed much higher anti-proliferative activity than cisplatin (IC_{50} = 8.2 ± 1.4 μM) against A549 cells, especially the complex $[Ru(dmp)_2(CAPIP)](ClO_4)_2$ (**Ru(II)-1**), which is 2-fold than cisplatin towards A549 cells. Thus, the complexes exhibits higher antitumor activity than ruthenium(II) complexes $(RuCl_2[L^a][DMSO]_2)\cdot H_2O$ (41.36 ± 0.99 μM) [49] and $[Ru(MeIm)_4(4mopip)]^{2+}$ (25.1 ± 0.6 μM) [50]. In addition, complexes **Ru(II)-1** and **Ru(II)-2** also shows moderate antitumor activity toward HepG-2, Hela and SGC-7901 cells and may be used as a potential broad-spectrum antineoplastic agents. Because the complexes **Ru(II)-1** and **Ru(II)-2** display excellent cytotoxic effect on the cell growth in A549, this cells were selected to perform the

following experiments.

3.3. Apoptosis assay with AO/EB and Annex V/PI double staining methods

To detect the preliminary mechanism of cell death induced by these Ru(II) complexes, AO/EB fluorescent staining assay was carried out for identification of live, apoptotic and necrotic cells [51]. AO is a crucial dye and stains both live and dead cells, whereas EB only stains cells that have lost membrane integrity and tinge the nucleus red [52]. Effect of Ru(II) complexes on the morphological changes of A549 cells is described in Fig. 1. Incubation different concentration of complexes **Ru(II)-1** (2.0 μM), **Ru(II)-2** (3.0 μM) for 24 h resulted in nuclear shrinkage, cell blebbing and chromatin condensation (Fig. 1 b, c), whereas no obvious change in cell nucleus and integrated cells was detected for the control cells (Fig. 1 a). The results indicated that the target complexes caused apoptosis of A549 cells.

To further quantitatively compare the effect of the Ru(II) complexes on the apoptosis, Annex V/PI double staining was used to investigate the percentage of apoptotic cells. The A549 cells were treated with different concentration of complexes **Ru(II)-1** (2.0 μM), **Ru(II)-2** (3.0 μM) for 24 h. Subsequently, the cells were harvested and stained with FITC Annex V and PI solutions respectively and the percentages of apoptotic cells were confirmed by flow cytometry. As described in Fig. 2, the percentage in the apoptosis (sum of early and late apoptosis cells) was increased in the presence of the **Ru(II)-1** and **Ru(II)-2** (2.91% for control group, 28.96% for **Ru(II)-1** and 22.25% for **Ru(II)-2**, respectively), and the apoptosis effects follow the

order **Ru(II)-1** > **Ru(II)-2**.

3.4. Intracellular reactive oxygen species levels determination

According to our previous report, Ru(II) polypyridyl complexes could induce an increase of reactive oxygen species (ROS). Moreover, ROS play a significant role in cancer cell apoptosis and autophagy [53,54]. With the aim to detect the effect of Ru(II) complexes on the cellular ROS production, A549 cells were treated for 24 h with **Ru(II)-1** and **Ru(II)-2**, or with Rosup for 30 min, used as positive control. We investigated the Ru(II)-induced ROS generation by the DCFH-DA. It is well known that DCFH-DA is oxidized by ROS to generate green fluorescent DCF (2′,7′-dichlorodihydrofluorescein diacetate). As shown from Fig. 3, in the control (a), no obvious green fluorescence could be detected. However, A549 cells were incubated with Rosup (b), different concentration of **Ru(II)-1** (2 μM, c) and **Ru(II)-2** (3 μM, d) for 24 h, a large amount of bright green fluorescent points were discovered. These date reveal that the Ru(II) complexes can enhance the intracellular ROS levels. Furthermore, the DCF fluorescent intensity was also investigated and described in Fig. 4. In the control, the DCF fluorescent intensity is 1.9. Treatment of A549 cells with different concentration of complexes **Ru(II)-1** (4.0 μM), **Ru(II)-1** (2.0 μM), **Ru(II)-2** (6.0 μM) and **Ru(II)-2** (3.0 μM), the fluorescent intensity are 40.3, 17.4, 44.7 and 20.3, respectively. Compared the results with the control, the fluorescent intensities of DCF grow 21.2, 9.2, 23.5 and 10.7 times than the original.

Superoxide anion ($O_2^{\bullet-}$) levels were investigated using DHE (Dihydroethidium) as

fluorescent reagent [55]. After freely passing through plasma membrane, non-fluorescent DHE oxidized by superoxide anion ($O_2^{\bullet-}$) to ethidium cation, which intercalates with DNA and stains nuclei bright red fluorescence [56]. As depicted in Fig. 5, in the control (a), no obvious red fluorescence could be detected. After A549 cells were incubated with different concentration of **Ru(II)-1** (2.0 μM, b), **Ru(II)-2** (3.0 μM, c) for 24 h, a number of red fluorescence was detected, implying that the **Ru(II)-1** and **Ru(II)-2** can increase intracellular superoxide anion levels, the red fluorescence intensity was detected by ImageXpress Micro XLS system and is described in Fig. 6, the red fluorescence intensity follows the order of **Ru(II)-1** > **Ru(II)-2**.

In addition, we examined nitric oxide (NO) production stimulated by **Ru(II)-1** and **Ru(II)-2** in A549 cells. DAF-FM DA was used as a fluorescent probe of NO. As depicted in Fig. 7, treatment of A549 cells (a) with different concentration of **Ru(II)-1** (2.0 μM) and **Ru(II)-2** (3.0 μM) for 24 h resulted in a significant enhance of green florescence. Moreover, the fluorescent intensity was also detected using ImageXpress Micro XLS system. As shown in Fig. 8, exposure of A549 cells to 4.0, 2.0, 6.0 and 3.0 μM of ruthenium(II) complexes led to an obvious enhance in green fluorescence intensity of 17.7 and 6.4 times for **Ru(II)-1**, 12.7 and 7.1 times for **Ru(II)-2** than that of control, respectively. The results demonstrate that **Ru(II)-1** and **Ru(II)-2** can increase the nitric oxide levels with a dose-dependent manner.

3.5. Location and changes of mitochondrial membrane potential

As one of the major subcellular structures, the significant function of mitochondria lies in that the mitochondria control the apoptotic signaling pathways and involved in many other cellular activities [11]. Therefore, to investigate whether the Ru(II) complexes targets to the mitochondria, A549 cells were treated with **Ru(II)-1** and **Ru(II)-2**, then the A549 cells were stained with Mito Tracker® Deep Green FM (ThermoFisher, 150 nM) and detected by ImageXpress Micro XLS system. As seen in Fig. 9, in the control (left, a, d), the mitochondria were stained in green. After A549 cells were exposed to 1.0 μM of **Ru(II)-1** and **Ru(II)-2** for 4 h (middle, b, e), Ru(II) complexes emitted bright red fluorescence. The pale yellow (right, c, f) detected from merge of green and red fluorescence images suggests that **Ru(II)-1** and **Ru(II)-2** targets the mitochondria [57].

The Ru(II) complexes can arrive the mitochondria and targets the mitochondria, this results stimulate us to test the changes of MMP (mitochondrial membrane potential, ΔΨm) [58]. The effects of Ru(II) complexes on the mitochondrial membrane potential of A549 cells was studied by detecting the red/green fluorescence of JC-1 by fluorescence microscope [59]. Normally, in normal cells, JC-1 exists as aggregates and emits red fluorescence (high ΔΨm), and when it is in apoptotic cells, it exists in a monomeric form to emit green fluorescence. As depicted in Fig. 10, in the control (a) JC-1 emits red fluorescence corresponding to high MMP. After A549 cells were exposed to CCCP (carbonylcyanide-m-chlorophenylhydrazone, b, positive control), complexes **Ru(II)-1** (2.0 μM, c) and **Ru(II)-2** (3.0 μM, d) for 24 h, JC-1 emits bright green fluorescence corresponding to low MMP. Therefore, the detected

data indicate that complexes **Ru(II)-1** and **Ru(II)-2** can induce destruction of mitochondrial membrane integrity and decrease MMP in A549 cells. In addition, the depolarization ratio of mitochondria was investigated by analyzing the fluorescent intensity of red/green value of JC-1 [60]. As seen in Fig. 11, in the control the ratio of red/green value is 0.94. After A549 cells were treated with CCCP (positive control) and different concentrations of **Ru(II)-1** (4.0 and 2.0 μM) and **Ru(II)-2** (6.0 and 3.0 μM) for 24 h, the ratios of the red/green values decrease significantly. It is further proved that the complexes **Ru(II)-1** and **Ru(II)-2** can induce the decrease of MMP.

3.6. Transwell cell migration and invasion assay

Malignant tumors have some significant characteristics, including the migratory and invasive abilities of cancer cells [61]. Therefore, it is essential to detect the effects of **Ru(II)-1** and **Ru(II)-2** on inhibiting the migration rate of A549 cells. The ability of the ruthenium complexes on cell invasion in A549 cells was detected by Boyden chamber invasion method. Detection results as shown in Fig. 12, and we can find that complexes **Ru(II)-1** and **Ru(II)-2** have obvious inhibitory effects on the invasion of A549 cells. To quantitatively compare the effect of different concentration of **Ru(II)-1** and **Ru(II)-2** on the cell invasion. As depicted in Fig. 13. A549 cells were treated with different concentration of complexes for 24 h, the percentage of inhibiting the cell invasion reaches 79.6% (**Ru(II)-1**, 4.0 μM), 43.4% (**Ru(II)-1**, 2.0 μM), 56.7% (**Ru(II)-2**, 6.0 μM) and 37.4% (**Ru(II)-2**, 3.0 μM), respectively. Notably, these two Ru(II) complexes displays a dose-dependent manner to inhibit the cell invasion.

3.7. Cell cycle arrest studies

Inhibition of malignant tumor proliferation by metal antitumor drugs could be the result of cell cycle arrest or induction of apoptosis [62,63]. To determine whether our Ru(II) complexes affect A549 cells proliferation by testing cell cycle distribution, DNA-based cell cycle analysis was carried out using flow cytometry. As shown in Fig. 14, in the control (a), the percentage in the cell cycle at S phase is 24.96%. After the A549 cells were treated with different concentration of Ru(II) complexes for 24 h, the percentages in the cell at S phase are 32.83% for **Ru(II)-1** (b) and 33.71% for **Ru(II)-2** (c), respectively. A noticeable increase of 7.87% for **Ru(II)-1** and 8.75% for **Ru(II)-2** in the percentages in the cells at S phase was obtained, accompanied by corresponding decline in the percentage in the cell at G_0/G_1 phase. The above results indicated that these two Ru(II) complexes induce A549 cell cycle arrest at the S phase. In addition, the percentage of cells in the sub-G_1-phase (Apo) increased from 0% in the control (a), to 32.76% (b) and 32.52% (c) in cells incubated with different concentration of Ru(II) complexes, respectively.

3.8. Complexes-CT DNA binding studies

Ru(II) polypyridyl complexes with special chemical structure are broadly documented to interact with DNA via noncovalent binding, and their antitumor activity is commonly considered to be related to their ability to bind to DNA [64]. Absorption spectra titration experiment is the significant path to study the binding mode of DNA with metal complexes by observing changes in absorption intensity and

position [65]. The absorption spectra of **Ru(II)-1** and **Ru(II)-2** in the absence and presence of increasing concentrations of CT DNA are illustrated in Fig. S1 (see the Supporting Information for details). With increasing the concentration of CT DNA, the metal-to-ligand charge transfer bonds of **Ru(II)-1** at 467 nm and **Ru(II)-2** at 469 nm exhibit clear hypochromism of about 25.4% and 15.1%, and bathochromism of 4 and 3 nm, respectively. The above results clearly show that the complexes **Ru(II)-1** and **Ru(II)-2** could interact with CT DNA through an intercalative mode. The K_b values of Ru(II) complexes are 6.12×10^5 M^{-1} (**Ru(II)-1**, 5 μM) and 5.07×10^5 M^{-1} (**Ru(II)-2**, 5 μM), respectively, which are less than that of the complexes **1** (2.1×10^6 M^{-1}), **2** (2.5×10^6 M^{-1}) and **3** (1.2×10^6 M^{-1}) [66], but were higher than that of complexes $[Ru(phen)_2bpym]^{2+}$ (ppym = *N*-[1,10]phenanthrolin-5-yl-pyrenylmethanimine, 1.2×10^5 M^{-1}) [67].

Moreover, viscosity investigation is broadly used to determine the binding mechanism between Ru(II) complexes and DNA [68]. It is popularly accepted that a classical intercalation of a ligand into DNA is known to cause a significant increase in the viscosity of a DNA solution due to an increase in the separation of the base pairs at the intercalation site [69]. Therefore, the intercalation pattern of the complexes with CT DNA can be judged by the changes of viscosity. Fig. 15 shows the effect of complexes **Ru(II)-1** and **Ru(II)-2** on the relative viscosity of CT DNA. On increasing the amount of complexes **Ru(II)-1** and **Ru(II)-2**, the viscosity values of the CT DNA increased steadily. The enhanced degree of the viscosity is in order of complexes **Ru(II)-1** > **Ru(II)-2**. These results indicated that complexes **Ru(II)-1** and **Ru(II)-2**

intercalate between the base pair of CT DNA.

4. Conclusions

In conclusion, we have designed and synthesized two novel fluorine and furan-substituted ruthenium polypyridyl complexes. An in vitro cytotoxicity assay indicated that complexes **Ru(II)-1** and **Ru(II)-2** can effectively inhibit A549 cells proliferation. The absorption spectra and viscosity investigation show that Ru(II) complexes interact with CT DNA through intercalative mode. Location assay of the complexes showed that target complexes enter into the mitochondria and lead to a decrease in the mitochondrial membrane potential. In addition, complexes **Ru(II)-1** and **Ru(II)-2** can induce A549 cells apoptosis and increase the intracellular reactive oxygen species levels in a concentration-dependent manner. Further anticancer mechanistic studies suggest that Ru(II) complexes inhibit the cell growth in A549 cells at S-phase. Moreover, the migration and invasion assay demonstrates that the complexes **Ru(II)-1** and **Ru(II)-2** can impede A549 cell migration. Thus, target Ru(II) complexes induce apoptosis of A549 cells through the ROS-mediated mitochondria dysfunction pathways, demonstrating that **Ru(II)-1** and **Ru(II)-2** could be a possible candidate for therapeutic application in malignant tumors.

Acknowledgements

The authors thank the Guangxi Natural Science Foundation (2018GXNSFBA050024), the Ph. D. Scientific Research Foundation of Guilin University of Technology, and Key Laboratory of Electrochemical and Magnetochemical Function Materials.

References

[1] X. Wang, Z. Guo, Targeting and delivery of platinum-based anticancer drugs, Chem. Soc. Rev. 42 (2013) 202-224.

[2] W.J. Rieter, K. M. Pott, K. M.L. Taylor, W. Lin, Nanoscale Coordination Polymers for Platinum-Based Anticancer Drug Delivery, J. Am. Chem. Soc. 130 (2008) 11584-11585.

[3] C. Brauckmann, C.A. Wehe, M. Kieshauer, C. Lanvers-Kaminsky, M. Sperling, U. Karst, The interaction of platinum-based drugs with native biologically relevant proteins, Anal. Bioanal. Chem. 405 (2013) 1855-1864.

[4] T. Sun, W. Cui, M. Yan, G. Qin, W. Guo, H. Gu, S. Liu, Q. Wu, Target Delivery of a Novel Antitumor Organoplatinum(IV)-Substituted Polyoxometalate Complex for Safer and More Effective Colorectal Cancer Therapy In Vivo, Adv. Mater. 28 (2016) 7397-7404.

[5] E. Wong, C.M. Giandomenico, Current Status of Platinum-Based Antitumor Drugs, Chem. Rev. 99 (1999) 2451-2466.

[6] U. Kalinowska-Lis, J. Ochocki, K. Matlawska-Wasowska, Trans geometry in platinum antitumor complexes, Coordin. Chem. Rev. 252 (2008) 1328-1345.

[7] M. Imran, W. Aybu, I.S. Butler, Z.U. Rehman, Photoactivated platinum-based anticancer drugs, Coordin. Chem. Rev. 376 (2018) 405-429.

[8] Z. Yue, H. Wang, D.J. Bowers, M. Gao, M. Stilgenbauer, F. Nielsen, J.T. Shelley, Y.-R. Zheng, Nanoparticles of metal-organic cages designed to encapsulate platinum-based anticancer agents, Dalton Trans. 47 (2018) 670-674.

[9] Z. Xu, H.M. Chan, C. Li, Z. Wang, M.-K. Tse, Z. Tong, G. Zhu, Synthesis, Structure, and Cytotoxicity of Oxaliplatin-Based Platinum(IV) Anticancer Prodrugs Bearing One Axial Fluoride, Inorg. Chem. 57 (2018) 8227-8235.

[10] W.-Y. Zhang, F. Du, M. He, L. Bai, Y.-Y. Gu, L.-L. Yang, Y.-J. Liu, Studies of anticancer activity in vitro and in vivo of iridium(III) polypyridyl complexes-loaded liposomes as drug delivery system, Eur. J. Med. Chem. 178 (2019) 390-400.

[11] W.-Y. Zhang, Yang.-J. Wang, F. Du, M. He, Y.-Y. Gu, L. Bai, L.-L. Yang, Y.-J. Liu, Evaluation of anticancer effect in vitro and in vivo of iridium(III) complexes on gastric carcinoma SGC-7901 cells, Eur. J. Med. Chem. 178 (2019) 401-416.

[12] T. Meng, Q.-P. Qin, Z.-L. Chen, H.-H. Zou, K. Wang, F.-P. Liang, High in vitro and in vivo antitumor activities of Ln(III) complexes with mixed 5,7-dichloro-2-methyl-8-quinolinol and 4,4′-dimethyl-2,2′-bipyridyl chelating ligands, Eur. J. Med. Chem. 169 (2019) 103-110.

[13] K. Laws, G. Bineva-Todd, A. Eskandari, C. Lu, N.O. Reilly, K. Suntharalingam, A Copper(II) Phenanthroline Metallopeptide That Targets and Disrupts Mitochondrial Function in Breast Cancer Stem Cells, Angew. Chem. Int. Ed. 57 (2017) 287-291.

[14] C. Lu, A. Eskandari, P.B. Cressey, K. Suntharalingam, Cancer Stem Cell and Bulk Cancer Cell Active Copper(II) Complexes with Vanillin Schiff Base Derivatives and Naproxen, Chem. Eur. J. 23 (2017) 11366-11374.

[15] V. Opletalová, D.S. Kalinowsk, M. Vejsová, J. Kuneš, M. Pour, J. Jampílek, V.

Buchta, D.R. Richardson, Identification and Characterization of Thiosemicarbazones with Antifungal and Antitumor Effects: Cellular Iron Chelation Mediating Cytotoxic Activity, Chem. Res. Toxicol. 21 (2008) 1878-1889.

[16] Y. Chao, G. Chen, C. Liang, J. Xu, Z. Dong, X. Han, C. Wang, Z. Liu, Iron Nanoparticles for Low-Power Local Magnetic Hyperthermia in Combination with Immune Checkpoint Blockade for Systemic Antitumor Therapy, Nano Lett. 19 (2019) 4287-4296.

[17] Y. Han, X. Liu, Z. Tian, X. Ge, J. Li, M. Gao, Y. Li, Y. Liu, Z. Liu, Half‐sandwich Iridium(III) Benzimidazole-Appended Imidazolium- Based *N*- heterocyclic Carbene Complexes and Antitumor Application, Chem. Asian J. 13 (2018) 3697-3705.

[18] J. Qi, S. Liang, Y. Gou, Z. Zhang, Z. Zhou, F. Yang, H. Liang, Synthesis of four binuclear copper (II) complexes: Structure, anticancer properties and anticancer mechanism, Eur. J. Med. Chem. 96 (2015) 360-368.

[19] Z. Yu, M. Han, J. Cowan, Toward the Design of a Catalytic Metallodrug: Selective Cleavage of G-Quadruplex Telomeric DNA by an Anticancer Copper-Acridine-ATCUN Complex, Angew. Chem. Int. Ed. 53 (2014) 1901-1905.

[20] Y.-Y. Qi, Q. Gan, Y.-X. Liu, Y.-H. Xiong, Z.-W. Mao, X.-Y. Le, Two new Cu(II) dipeptide complexes based on 5-methyl-2-(2′-pyridyl)benzimidazole as potential antimicrobial and anticancer drugs: Special exploration of their possible anticancer mechanism, Eur. J. Med. Chem. 154 (2018) 220-232.

[21] L. Xie, Z. Luo, Z. Zhao, T. Chen, Anticancer and antiangiogenic iron (II) complexes that target thioredoxin reductase to trigger cancer cell apoptosis, J. Med. Chem. 60 (2017) 202-214.

[22] G.-B. Jiang, W.-Y. Zhang, M. He, Y.-Y. Gu, L. Bai, Y.-J. Wang, Q.-Y. Yi, F. Du, Anticancer activity of two ruthenium(II) polypyridyl complexes toward Hepatocellular carcinoma HepG-2 cells, Poly. 169 (2019) 209-218.

[23] J.-Q. Wang, P.-Y. Zhang, L.-N. Ji, H. Chao, A ruthenium(II) complex inhibits tumor growth in vivo with fewer side-effects compared with cisplatin, J. Inorg. Biochem. 146 (2015) 89-96.

[24] L. Lakomska, M. Fandzloch, T. Muziol, T. Lis, J. Jezierska, Synthesis, characterization and antitumor properties of two highly cytotoxic ruthenium(III) complexes with bulky triazolopyrimidine ligands, Dalton Trans. 42 (2013) 6219-6226.

[25] V.B. Arion, A. Dobrov, S. Göschl, M.A. Jakupec, B.K. Keppler, P. Rapta, Ruthenium- and osmium-arene-based paullones bearing a TEMPO free-radical unit as potential anticancer drugs, Chem. Commun. 48 (2012) 8559-8561.

[26] A. Koceva-Chyła, K. Matczak, M.P. Hikisz, M.K. Durka, M.K. Kochel, G. Süss-Fink, J. Furrer, K. Kowalski, Insights into the in vitro Anticancer Effects of Diruthenium-1, ChemMedChem 11 (2016) 2171-2187.

[27] G. Petruk, D.M. Monti, G. Ferraro, A. Pica, L. D'Elia, F. Pane, A. Amoresano, J. Furrer, K. Kowalski, A. Merlino, Encapsulation of the Dinuclear Trithiolato-Bridged Arene Ruthenium Complex Diruthenium-1 in an Apoferritin

Nanocage: Structure and Cytotoxicity, ChemMedChem 14 (2019) 594-602.

[28] J. Liu, H. Lai, Z. Xiong, B. Chen, T. Chen, Functionalization and cancer-targeting design of ruthenium complexes for precise cancer therapy, Chem. Commun. 55 (2019) 9904-9914.

[29] A. Weiss, R.H. Berndsen, M. Dubois, C. Müller, R. Schibli, A.W. Griffioen, P.J. Dyson, P. Nowak-Sliwinska, In vivo anti-tumor activity of the organometallic ruthenium(II)-arene complex [Ru(η^6-p-cymene)Cl_2(pta)] (RAPTA-C) in human ovarian and colorectal carcinomas, Chem. Sci. 5 (2014) 4742-4748.

[30] D. Wan, B. Tang, Y.-J. Wang, B.-H. Guo, H. Yin, Q.-Y. Yi, Y.-J. Liu, Synthesis and anticancer properties of ruthenium (II) complexes as potent apoptosis inducers through mitochondrial disruption, Eur. J. Med. Chem. 139 (2018) 180-190.

[31] Y. Zhang, A. Ho, J. Yue, L. Kong, Z. Zhou, X. Wu, F. Yang, H. Liang, Structural basis and anticancer properties of ruthenium-based drug complexed with human serum albumin, Eur. J. Med. Chem. 86 (2014) 449-455.

[32] G.-B. Jiang, W.-Y. Zhang, M. He, Y.-Y. Gu, L. Bai, Y.-J. Wang, Q.-Y. Yi, F. Du, Design and synthesis of new ruthenium polypyridyl complexes with potent antitumor activity in vitro, Spectrochim. Acta. A Mol. Biomol. Spectrosc. 220 (2019) 117132-117143.

[33] C.G. Mortimer, G. Wells, J.-P. Crochard, E.L. Stone, T.D. Bradshaw, M.F.G. Stevens, A.D. Westwell, Antitumor Benzothiazoles. 26. 2-(3,4-Dimethoxyphenyl)-5-fluorobenzothiazole (GW 610, NSC 721648), a Simple Fluorinated 2-Arylbenzothiazole, Shows Potent and Selective Inhibitory

Activity against Lung, Colon, and Breast Cancer Cell Lines, J. Med. Chem. 49 (2006) 179-185.

[34] M.M. Fouad, E.R. EI-Bendary, G.M. Suddek, I.A. Shehata, M.M. EI-Kerdawy, Synthesis and in vitro antitumor evaluation of some new thiophenes and thieno[2,3-d]pyrimidine derivatives, Bioorgan. Chem. 81 (2018) 587-598.

[35] S. Wei, L. Li, Y. Shu, K. Zhao, Z. Ji, Synthesis, antifungal and antitumor activity of two new types of imidazolin-2-ones, Bioorg. Med. Chem. 25 (2017) 6501-6510.

[36] I.M. Abdou, A.M. Saleh, H.F. Zohdi, Synthesis and Antitumor Activity of 5-Trifluoromethyl-2,4-dihydropyrazol-3-one Nucleosides, Molecules. 9 (2004) 109-116.

[37] W. Paw, R. Eisenberg, Synthesis, Characterization, and Spectroscopy of Dipyridocatecholate Complexes of Platinum, Inorg. Chem. 36 (1997) 2287-2293.

[38] B. Tang, D. Wan, S.-H. Lai, H.-H. Yang, C. Zhang, X.-Z. Wang, C.-C. Zeng, Y.-J. Liu, Design, synthesis and evaluation of anticancer activity of ruthenium (II) polypyridyl complexes, J. Inorg. Biochem. 173 (2017) 93-104.

[39] L. Perdisatt, S. Moqadasi, L. O′Neill, G, Hessman, A. Ghion, M.Q.M. Warraich, A. Casey, C. O′Connor, Synthesis, characterisation and DNA intercalation studies of regioisomers of ruthenium (II) polypyridyl complexes, J. Inorg. Biochem. 182 (2018) 71-82.

[40] J. Marmur, A procedure for the isolation of deoxyribonucleic acid from micro-organisms, J. Mol. Biol. 3 (1961) 208-218.

[41] M.E. Reichmann, S.A. Rice, C.A. Thomas, P. Doty, A further examination of the molecular weight and size of desoxypentose nucleic acid, J. Am. Chem. Soc. 76 (1954) 3047-3053.

[42] A. Wolf, G.H. Shimer, T. Meehan, Polycyclic aromatic hydrocarbons physically intercalate into duplex regions of denatured DNA, Biochemistry. 26 (1987) 6392-6396.

[43] J.B. Chaires, N. Dattagupta, D.M. Crothers, Studies on interaction of anthracycline antibiotics and deoxyribonucleic acid: equilibrium binding studies on the interaction of daunomycin with deoxyribonucleic acid, Biochemistry. 21 (1982) 3933-3940.

[44] S. Satyanarayana, J.C. Dabrowiak, J.B. Chaires, Tris (phenanthroline) ruthenium (II) enantiomer interactions with DNA: mode and specificity of binding, Biochemistry. 32 (1993) 2573-2584.

[45] S. Satyanaryana, J.C. Dabrowial, J.B. Chaires, Neither .DELTA.- nor .LAMBDA.-tris(phenanthroline)ruthenium(II) binds to DNA by classical intercalation, Biochemistry. 31 (1992) 9319-9324.

[46] G. Cohen, H. Eisenberg, Viscosity and sedimentation study of sonicated DNA-proflavine complexes, Biopolymers. 8 (1969) 45-55.

[47] S.D.A. Abel, S.K. Baird, Honey is cytotoxic towards prostate cancer cells but interacts with the MTT reagent: Considerations for the choice of cell viability assay, Food. Chem. 241 (2018) 70-78.

[48] B. Kadriye, T. Yagmur, C. Zerrin, A. Oge, A. Filiz, Cytotoxic and genotoxic

effects of $[Ru(phi)_3]^{2+}$ evaluated by Ames/Salmonella and MTT methods, Eur. J. Med. Chem. 44 (2009) 2601-2605.

[49] Q.-P. Qin, Z.-F. Wang, X.-L. Huang, M.-X. Tan, B.-B. Shi, H. Liang, High in Vitro and in Vivo Tumor-Selective Novel Ruthenium(II) Complexes with 3□(2′-Benzimidazolyl)-7-fluoro-coumarin, ACS Med. Chem. Lett. 10 (2019) 936-940.

[50] J. Chen, Y. Zhang, G. Li, F. Peng, x. Jie, J. She, G. Dongye, Z. Zou, S. Rong, L. Chen, Cytotoxicity in vitro, cellular uptake, localization and apoptotic mechanism studies induced by ruthenium(II) complex, J. Biol. Inorg. Chem. 23 (2018) 261-275.

[51] G. Jiang, X. Zheng, J.H. Yao, B. Han, W. Li, J. Wang, H. Huang, Y. Liu, Ruthenium (II) polypyridyl complexes induce BEL-7402 cell apoptosis by ROS-mediated mitochondrial pathway, J. Inorg. Biochem. 141 (2014) 170-179.

[52] B.A. Dar, A.M. Lone, W.A. Shah, M.A. Qurishi, Synthesis and screening of ursolic acid-benzylidine derivatives as potential anti-cancer agents, Eur. J. Med. Chem. 111 (2016) 26-32.

[53] D. Lacopetta, A. Mariconda, C. Saturnino, A. Caruso, G. Palma, J. Ceramella, N. Muià, M. Perri, M.S. Sinicropi, M.C. Caroleo, P. Longo, Novel Gold and Silver Carbene Complexes Exert Antitumor Effects Triggering the Reactive Oxygen Species Dependent Intrinsic Apoptotic Pathway, ChemMedChem. 12 (2017) 2054-2065.

[54] Y. Gou, J. Wang, S. Chen, Z. Zhang, Y. Zhang, W. Zhang, F. Yang,

α-*N*-heterocyclic thiosemicarbazone Fe(III) complex: Characterization of its antitumor activity and identification of anticancer mechanism, Eur. J. Med. Chem. 123 (2016) 354-364.

[55] H. Karlsson, M. Fryknäs, S. Strese, J. Gullbo, G. Westman, U. Bremberg, T. Sjöblom, T. Pandzic, R. Larsson, P. Nygren, Mechanistic characterization of a copper containing thiosemicarbazone with potent antitumor activity, Oncotarget. 8 (2017) 30217-30234.

[56] D. Deeb, X. Gao, H. Jiang, B. Janic, A.S. Arbab, Y. Rojanasakul, S. A. Dulchavsky, S.C. Gautam, Oleanane triterpenoid CDDO-Me inhibits growth and induces apoptosis in prostate cancer cells through a ROS-dependent mechanism, Biochem. Pharmaco. 79 (2010) 350-360.

[57] B. Tang, D. Wan, Y.-J. Wang, Q.-Y. Yi, B.-H. Guo, Y.-J. Liu, An iridium (III) complex as potent anticancer agent induces apoptosis and autophagy in B16 cells through inhibition of the AKT/mTOR pathway, Eur. J. Med. Chem. 145 (2018) 302-314.

[58] J.J. Li, L.H. Guo, Z.Z. Tian, S.M. Zhang, Z.S. Xu, Y.L. Han, R.X. Li, Y. Li, Z. Liu, Inorg. Chem. 57 (2018) 13552-13563.

[59] B. Peña, S. Saha, R. Barhoumi, R. C. Burghardt, K. R. Dunbar, Inorg. Chem. 57 (2018) 12777-12786.

[60] J. Marmur, A procedure for the isolation of deoxyribonucleic acid from micro-organisms, J. Mol. Biol. 3 (1961) 208-218.

[61] Y. Lu, T. Shen, H. Yang, W. Gu, Ruthenium Complexes Induce HepG2 Human

Hepatocellular Carcinoma Cell Apoptosis and Inhibit Cell Migration and Invasion through Regulation of the Nrf2 Pathway, Int. J. Mol. Sci. 17 (2016) 775-785.

[62] S. Xu, H. Yao, S. Luo, Y.-K. Zhang, D.-H. Yang, D. Li, G. Wang, M. Hu, Y. Qiu, X. Wu, H. Yao, W. Xie, Z.-S. Chen, J. Xu, A Novel Potent Anticancer Compound Optimized from a Natural Oridonin Scaffold Induces Apoptosis and Cell Cycle Arrest through the Mitochondrial Pathway, J. Med. Chem. 60 (2017) 1449-1468.

[63] D. Kong, M. Tian, L. Guo, X. Liu, S. Zhang, Y. Song, X. Meng, S. Wu, L. Zhang, Z. Liu, Novel iridium(III) iminopyridine complexes: synthetic, catalytic, and in vitro anticancer activity studies, J. Biol. Inorg. Chem. 23 (2018) 819-832.

[64] J. Du, Y. Kang, Y. Zhao, W. Zheng, Y. Zhang, Y. Lin, Z. Wang, Y. Wang, Q. Luo, K. Wu, F. Wang, Synthesis, Characterization, and in Vitro Antitumor Activity of Ruthenium(II) Polypyridyl Complexes Tethering EGFR-Inhibiting 4□Anilinoquinazolines, Inorg. Chem. 55 (2016) 4595-4605.

[65] H. Shi, G. Clarkson, P.J. Sadler, Dual action photosensitive platinum(II) anticancer prodrugs with photoreleasable azide ligands, Inorganica. Chimica. Acta. 489 (2019) 230-235.

[66] P. Liu, B.-Y. Wu, J. Liu, Y.-C. Dai, Y.-J. Wang, K.-Z. Wang, DNA Binding and Photocleavage Properties, Cellular Uptake and Localization, and in-Vitro Cytotoxicity of Dinuclear Ruthenium(II) Complexes with Varying Lengths in Bridging Alkyl Linkers, Inorg. Chem. 55 (2016), 1412-1422.

[67] M. Mariappan, A. Ramasamy, P.A. Prasanth, V. Anbazhagan, R. Senthilnathan, A. Jothi, Synthesis, solvatochromism, photochemistry, DNA binding, photocleavage,

cytotoxicity and molecular docking studies of a ruthenium(II) complex bearing photoactive subunit, J Photochem Photobio A. 132 (2014) 111-123.

[68] A. Srishailam, N.M. Gabra, Y.P. Kumar, K.L. Reddy, C.S. Devi, D.A. Kumar, S.S. Singh, S. Satyanarayana, Synthesis, characterization; DNA binding and antitumor activity of ruthenium(II) polypyridyl complexes, J Photochem Photobiol B Biol. 141 (2014) 47-58.

[69] H.S. Derrat, C.C. Robertson, A.J.H. Meijer, J.A. Thomas, Turning intercalators into groove binders: synthesis, photophysics and DNA binding properties of tetracationic mononuclear ruthenium(II)-based chromophore-quencher complexes, Dalton Trans. 47 (2018) 12300-12307.

Captions for Schemes and Figures

Scheme 1 The synthetic route of ligand and ruthenium(II) complexes.

Fig. 1 A549 cells were stained with AO/EB and detected under fluorescent microscope. A549 (a) exposed to different concentration of **Ru(II)-1** (2.0 μM) and **Ru(II)-2** (3.0 μM) for 24 h.

Fig. 2 Apoptosis was assayed with Annex V/PI staining A549 cells (a) in the presence of **Ru(II)-1** (2.0 μM, b) and **Ru(II)-2** (3.0 μM, c) for 24 h.

Fig. 3 Intracellular ROS was detected in A549 cells (a) exposure to Rosup (b, positive control), different concentration of **Ru(II)-1** (2.0 μM, c) and **Ru(II)-2** (3.0 μM, d) for 24 h.

Fig. 4 The DCF fluorescent intensity was determined after A549 cells treated with

different concentration of **Ru(II)-1** (4.0 and 2.0 μM) and **Ru(II)-2** (6.0 and 3.0 μM) for 24 h.

Fig. 5 The superoxide anion level was assayed after 24 h of A549 cells (a) with different concentration of **Ru(II)-1** (2.0 μM, b), **Ru(II)-2** (3.0 μM, c) and the cells were stained with DHE.

Fig. 6 The DHE fluorescent intensity was determined after A549 cells treated with different concentration of **Ru(II)-1** and **Ru(II)-2** for 24 h.

Fig. 7 The intracellular NO levels were detected after A549 cells (a) were exposed to different concentration of **Ru(II)-1** (2.0 μM, b) and **Ru(II)-2** (3.0 μM, c) for 24 h.

Fig. 8 The DAF-FMDA fluorescent intensity induced by the complexes was determined by ImageXpress Micro XLS system. $^{*}P < 0.05$ represents significant differences compared with control.

Fig. 9 Location of complexes in the mitochondria in A549 cell exposure to 1.0 μM of complexes **Ru(II)-1** and **Ru(II)-2** for 4 h.

Fig. 10 The changes of mitochondrial membrane potential was studied after A549 cells (a) were treated with CCCP (b), different concentration of complexes **Ru(II)-1** (2.0 μM, c), **Ru(II)-2** (3.0 μM, d) for 24 h and the cells were imaged under a fluorescent microscope.

Fig. 11 The ratio of the red/green fluorescent intensity was determined after A549 cells were treated with different concentration of **Ru(II)-1** (4.0 and 2.0 μM) and **Ru(II)-2** (6.0 and 3.0 μM) for 24 h. $^{*}P < 0.05$ represents significant

differences compared with control.

Fig. 12 Microscope images of invading A549 cells (a) induced by different concentration of **Ru(II)-1** (2.0 μM, b) and **Ru(II)-2** (3.0 μM, c) for 24 h.

Fig. 13 Percentage of inhibiting invasion of A549 cells induced by different concentration of **Ru(II)-1** (4.0 and 2.0 μM) and **Ru(II)-2** (6.0 and 3.0 μM) for 24 h. $^{*}P < 0.05$ represents significant differences compared with control.

Fig. 14 The cell cycle arrest in A549 cells were detected after A549 cells (a) were exposed to different concentration of **Ru(II)-1** (2.0 μM, b) and **Ru(II)-2** (3.0 μM, c) for 24 h.

Fig. 15 The effect of increasing the amounts of the **Ru(II)-1** and **Ru(II)-2** on the relative viscosity of CT DNA at 25 (± 0.1) ^{o}C. [DNA] = 0.25 mM.

Table 1 IC_{50} (μM) values of ligand and **[Ru]** complexes toward the selected cell lines.

complex	A549	HepG-2	SGC-7901	Hela
CAPIP	>100	>100	>100	>100
CFPIP	>100	>100	>100	>100
Ru(II)-1	4.1 ± 1.4	>100	27.0 ± 2.6	24.2 ± 2.2
Ru(II)-2	6.1 ± 1.6	18.9 ± 2.2	38.5 ± 3.2	17.9 ± 1.8
Cisplatin	8.2 ± 1.4	26.4 ± 2.6	4.4 ± 1.3	8.3 ± 1.1

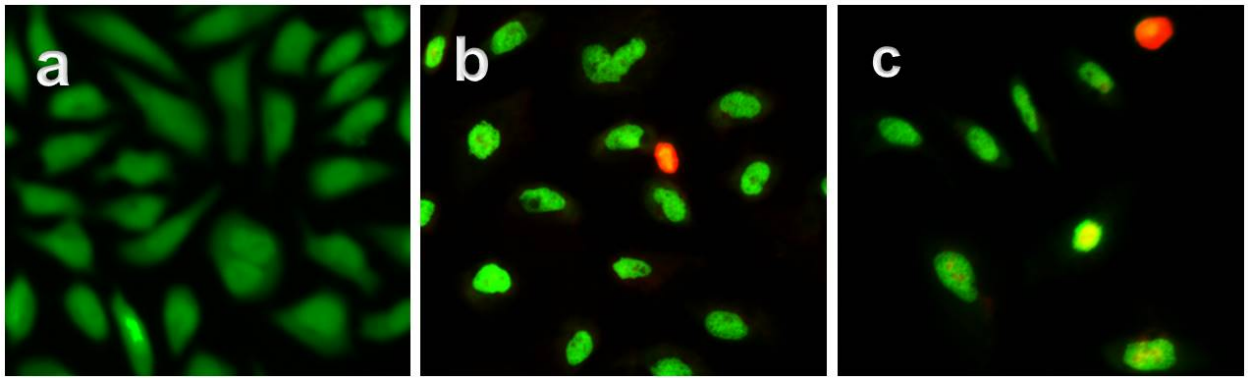

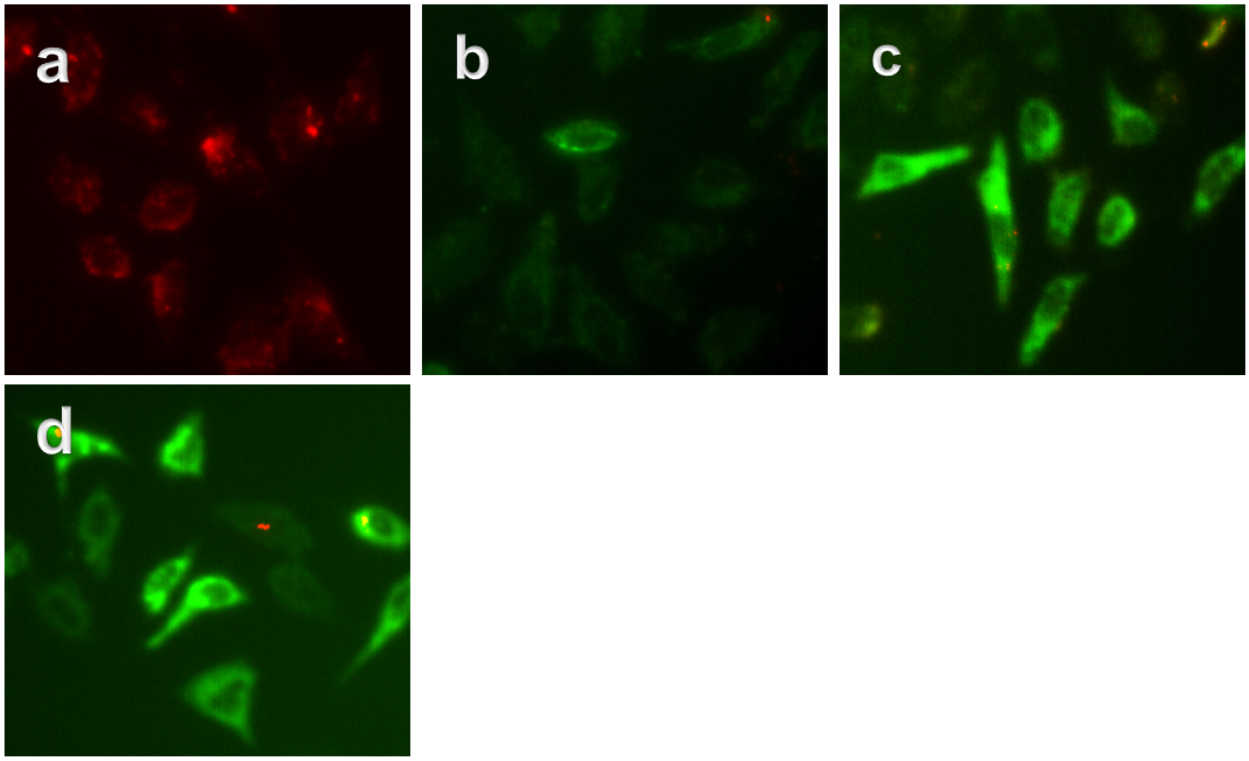

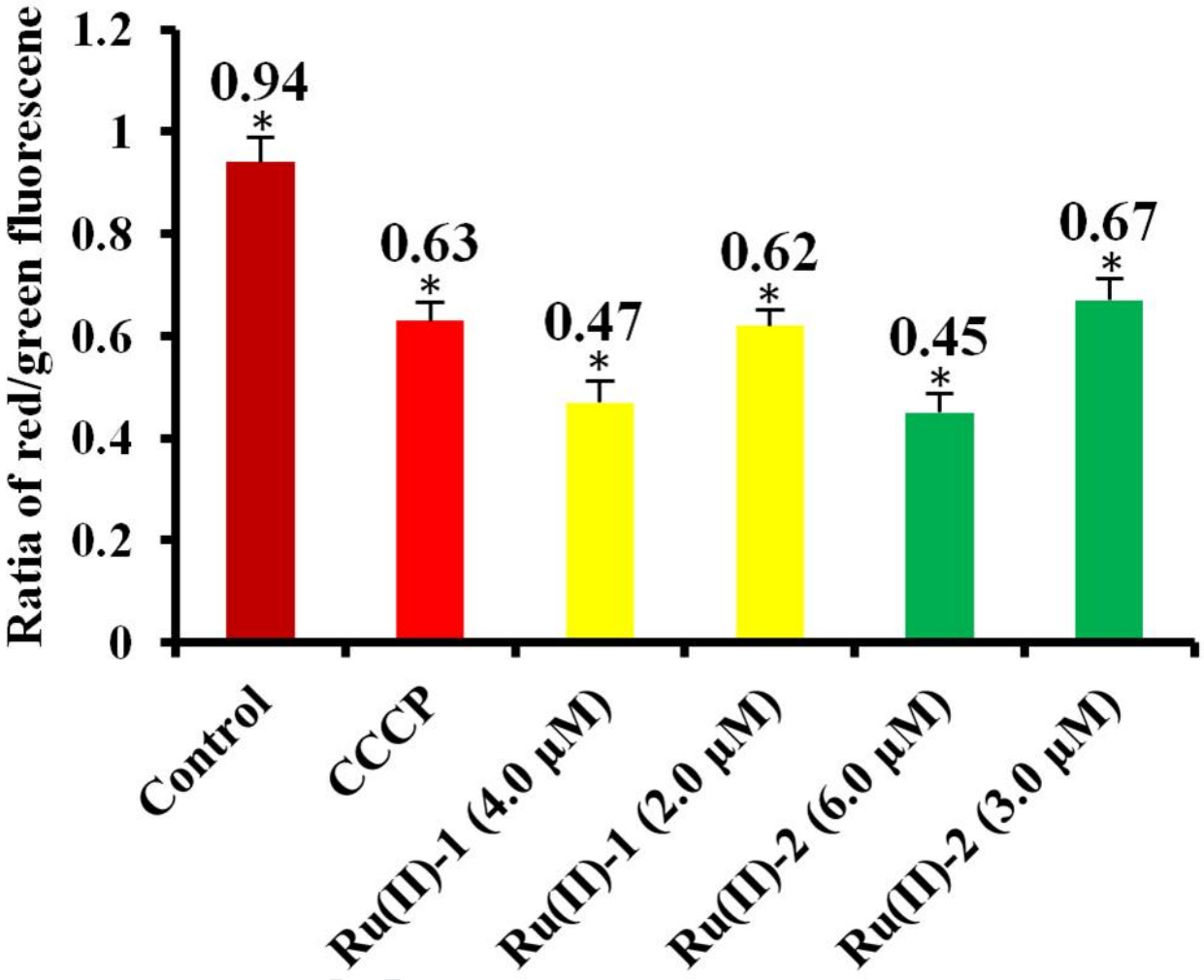
Ratia of red/green fluorescene
1.2
1
0.8
0.6
0.4
0.2
0
0.94
*
0.63
*
0.47
*
0.62
*
0.45
*
0.67
*
Control
CCCP
Ru(II)-1 (4.0 μM)
Ru(II)-1 (2.0 μM)
Ru(II)-2 (6.0 μM)
Ru(II)-2 (3.0 μM)

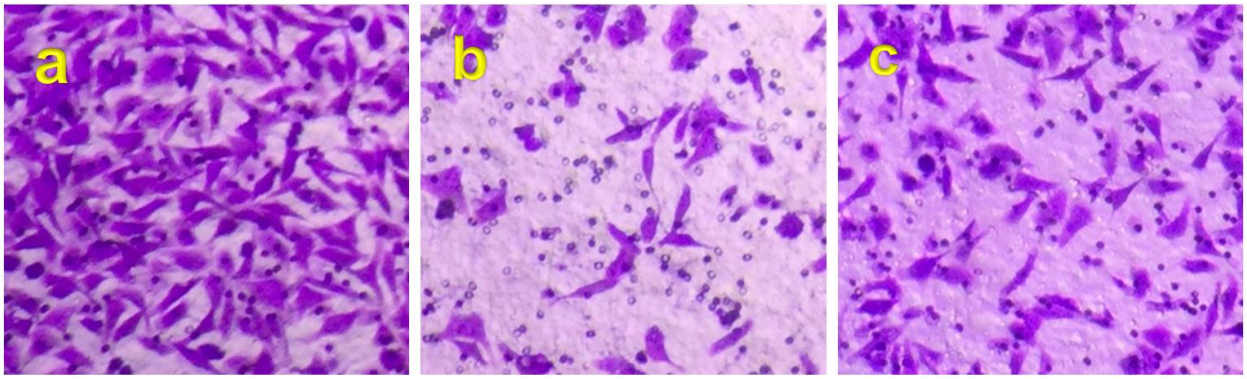

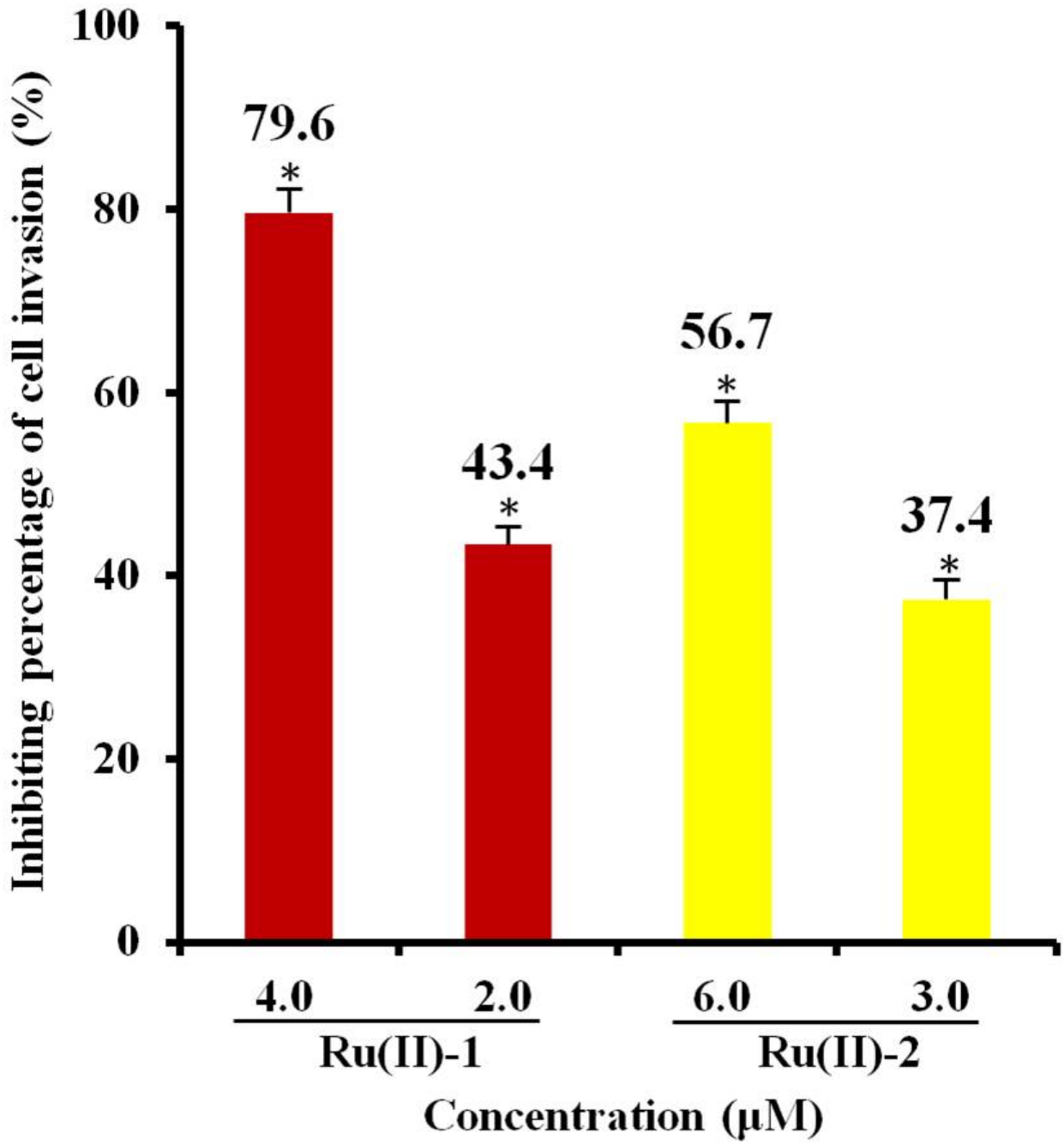
Inhibiting percentage of cell invasion (%)
100
80
60
40
20
0
79.6
*
43.4
*
56.7
*
37.4
*
4.0
2.0
6.0
3.0
Ru(II)-1
Ru(II)-2
Concentration (μM)

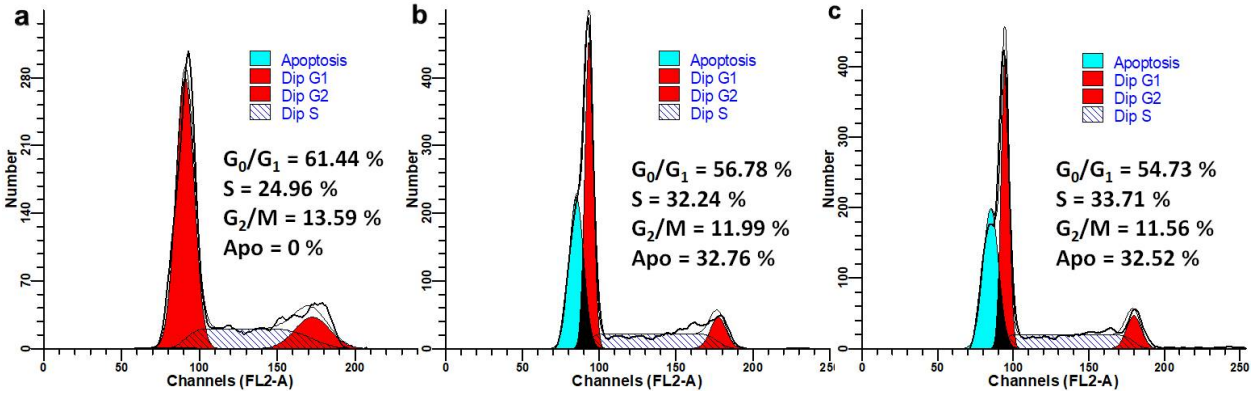

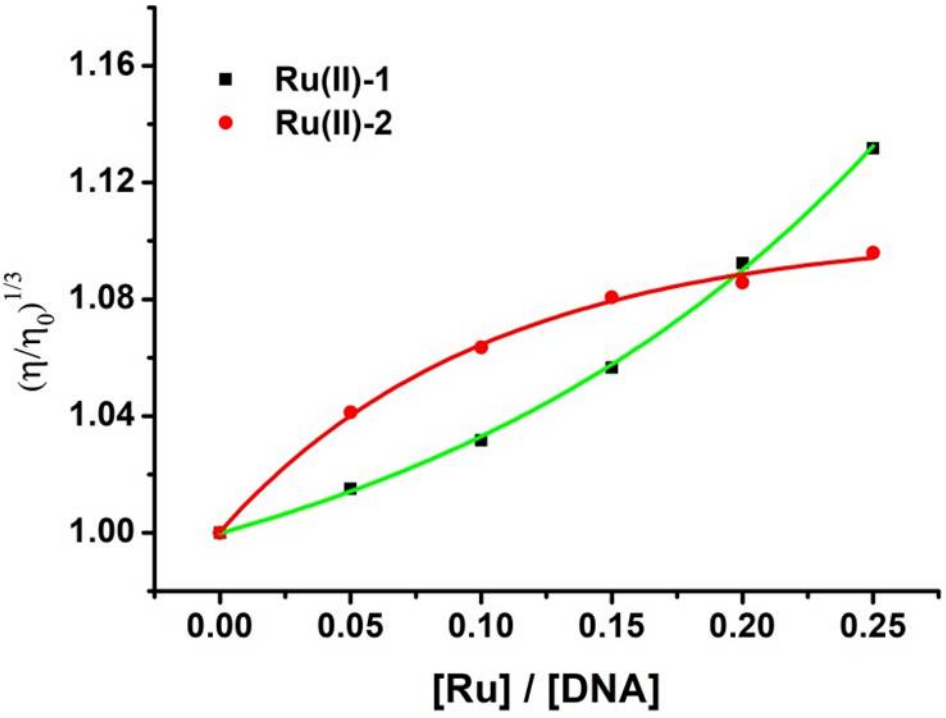

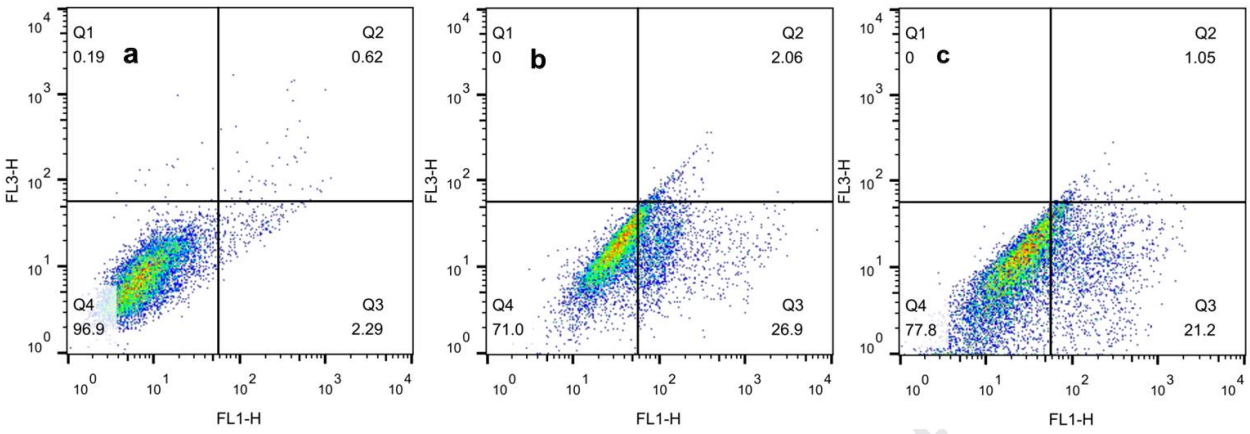

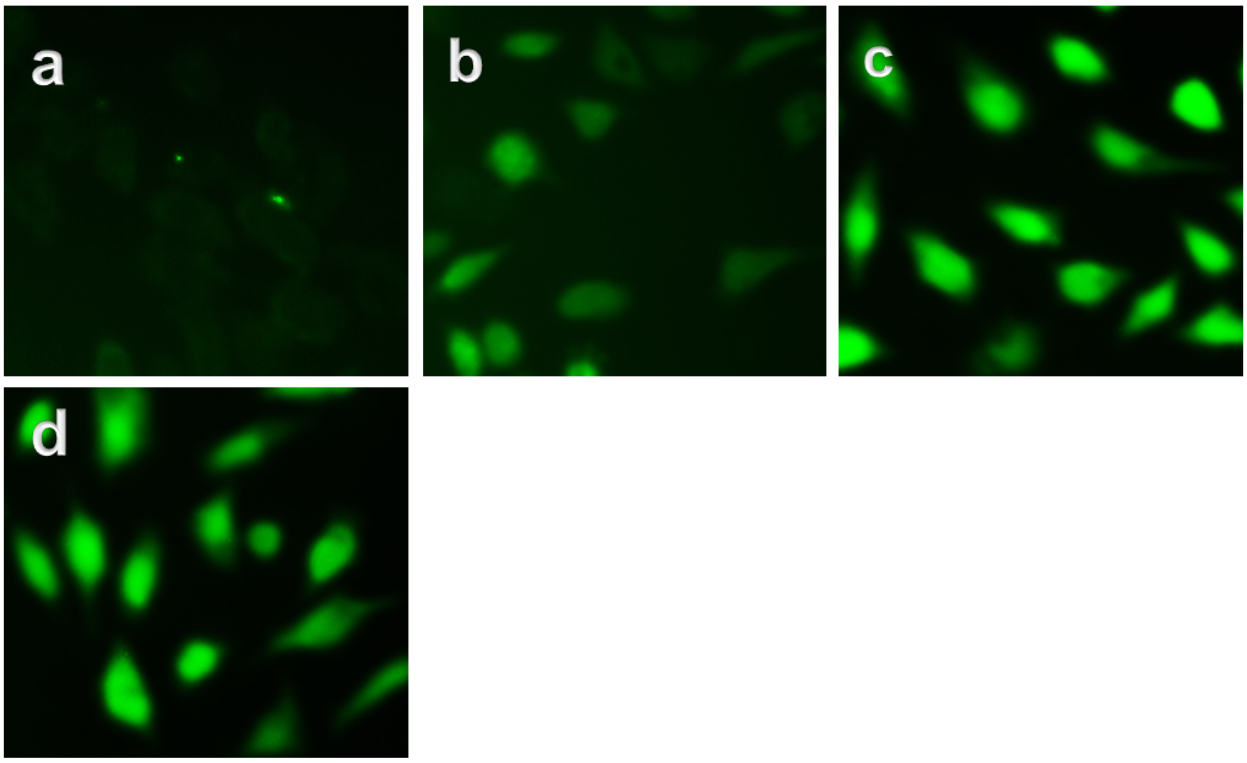

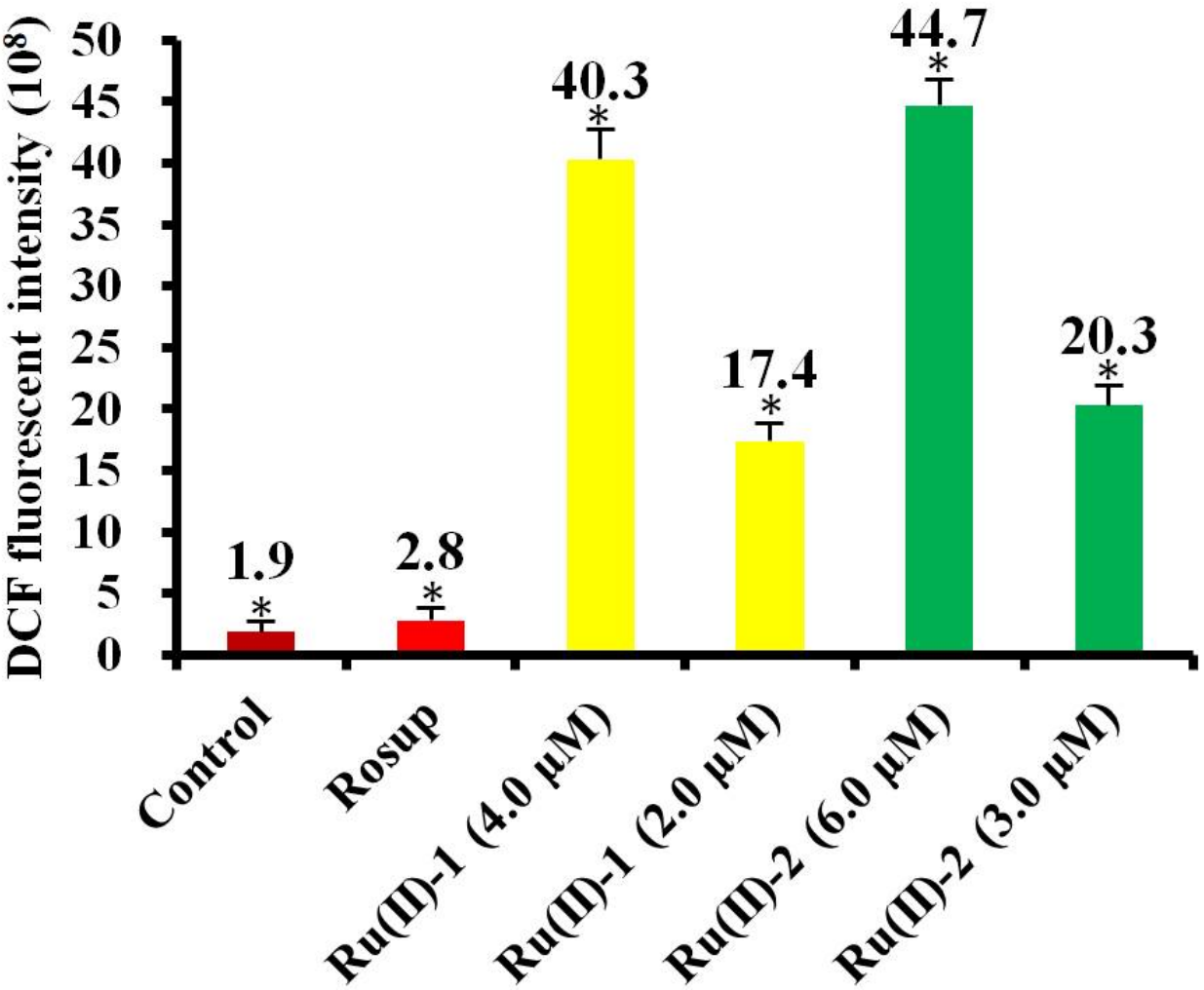
DCF fluorescent intensity (10^8)
50
45
40
35
30
25
20
15
10
5
0
1.9
*
2.8
*
40.3
*
17.4
*
44.7
*
20.3
*
Control
Rosup
Ru(II)-1 (4.0 μM)
Ru(II)-1 (2.0 μM)
Ru(II)-2 (6.0 μM)
Ru(II)-2 (3.0 μM)

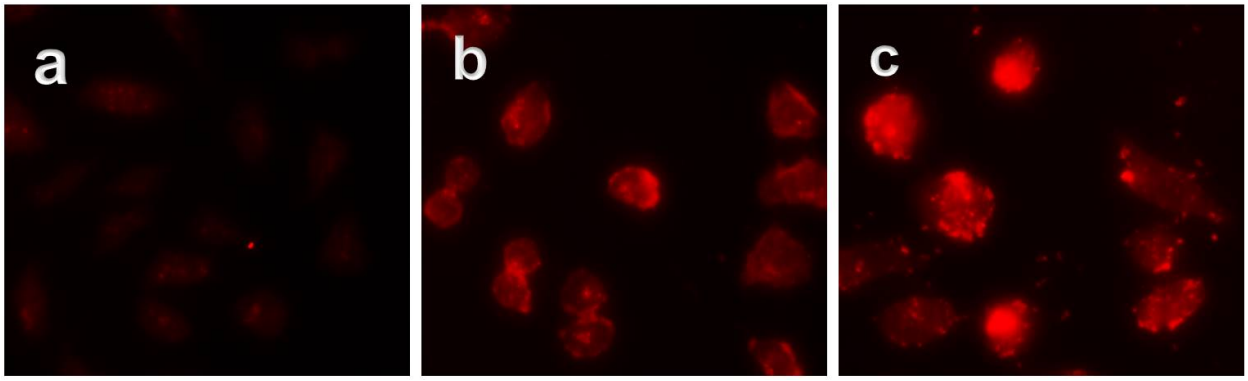

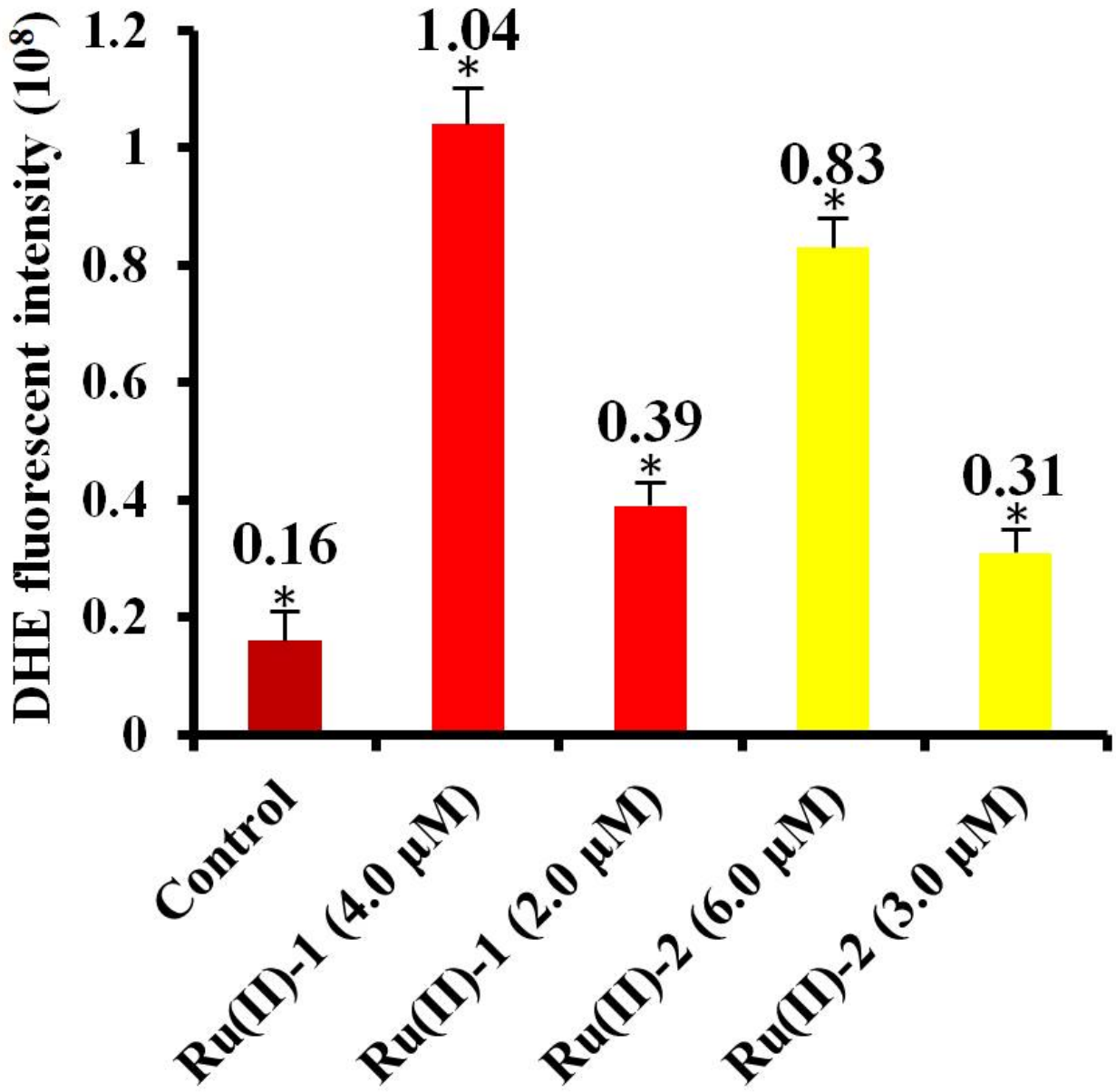
DHE fluorescent intensity (10^8)
1.2
1
0.8
0.6
0.4
0.2
0
0.16
1.04
0.39
0.83
0.31
*
Control
Ru(II)-1 (4.0 μM)
Ru(II)-1 (2.0 μM)
Ru(II)-2 (6.0 μM)
Ru(II)-2 (3.0 μM)

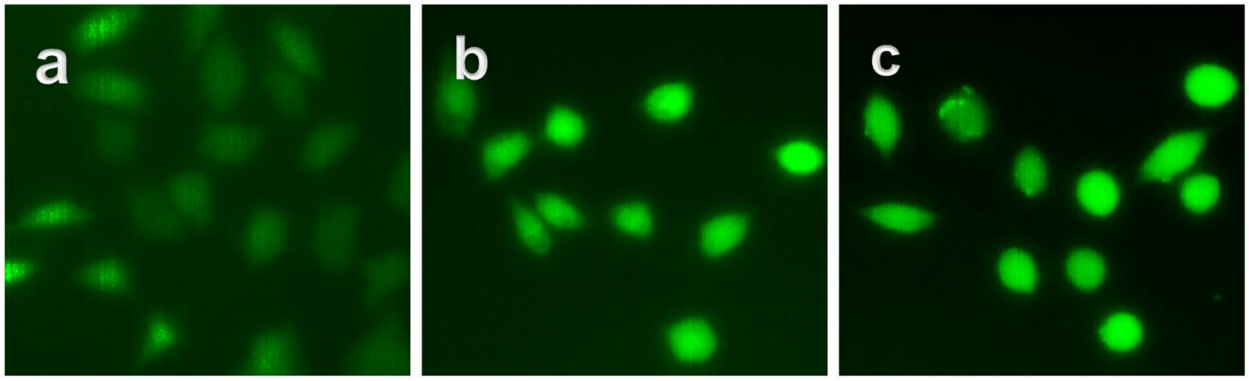

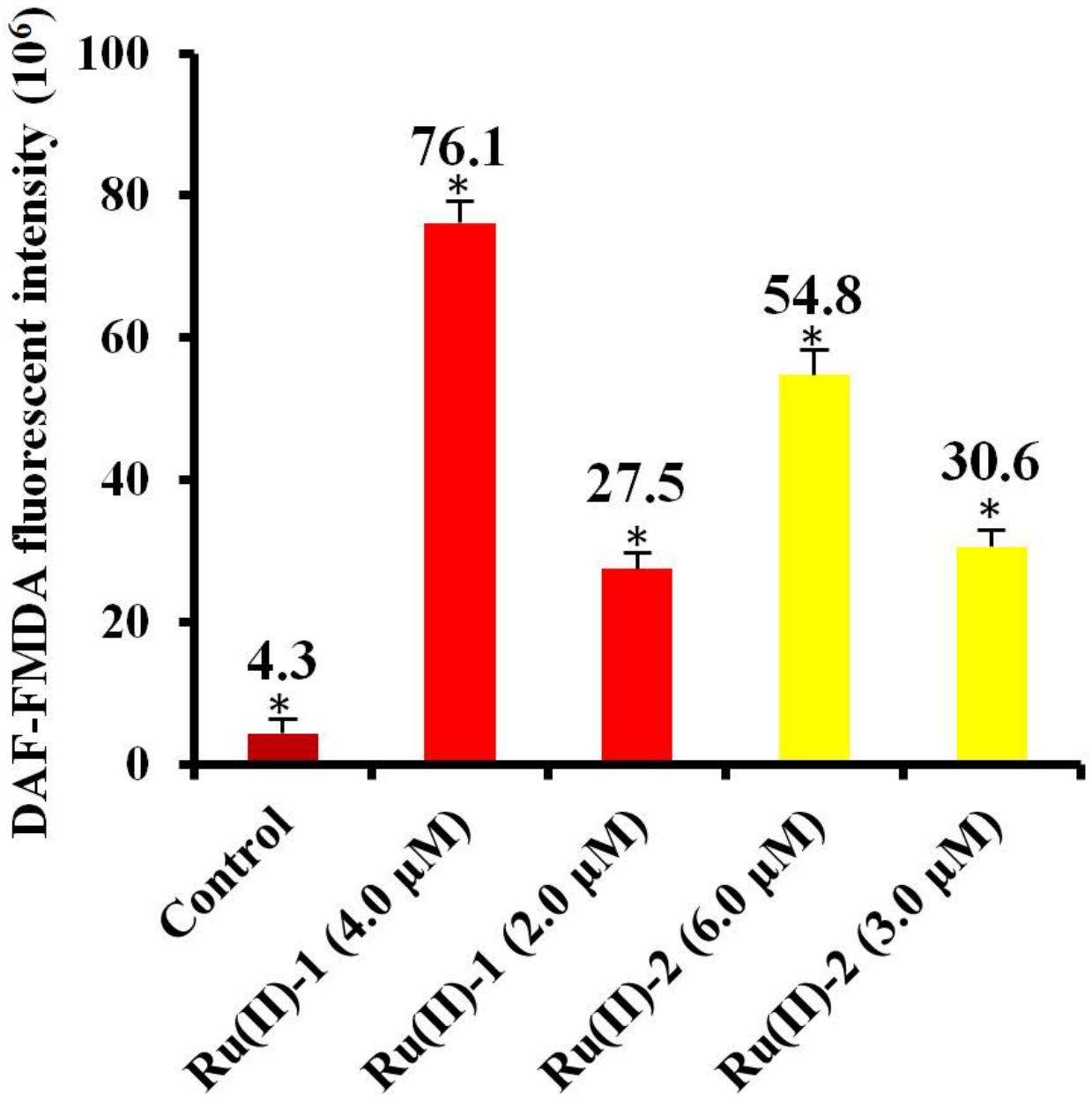
DAF-FMDA fluorescent intensity (10^6)
100
80
60
40
20
0
4.3
*
76.1
*
27.5
*
54.8
*
30.6
*
Control
Ru(II)-1 (4.0 μM)
Ru(II)-1 (2.0 μM)
Ru(II)-2 (6.0 μM)
Ru(II)-2 (3.0 μM)

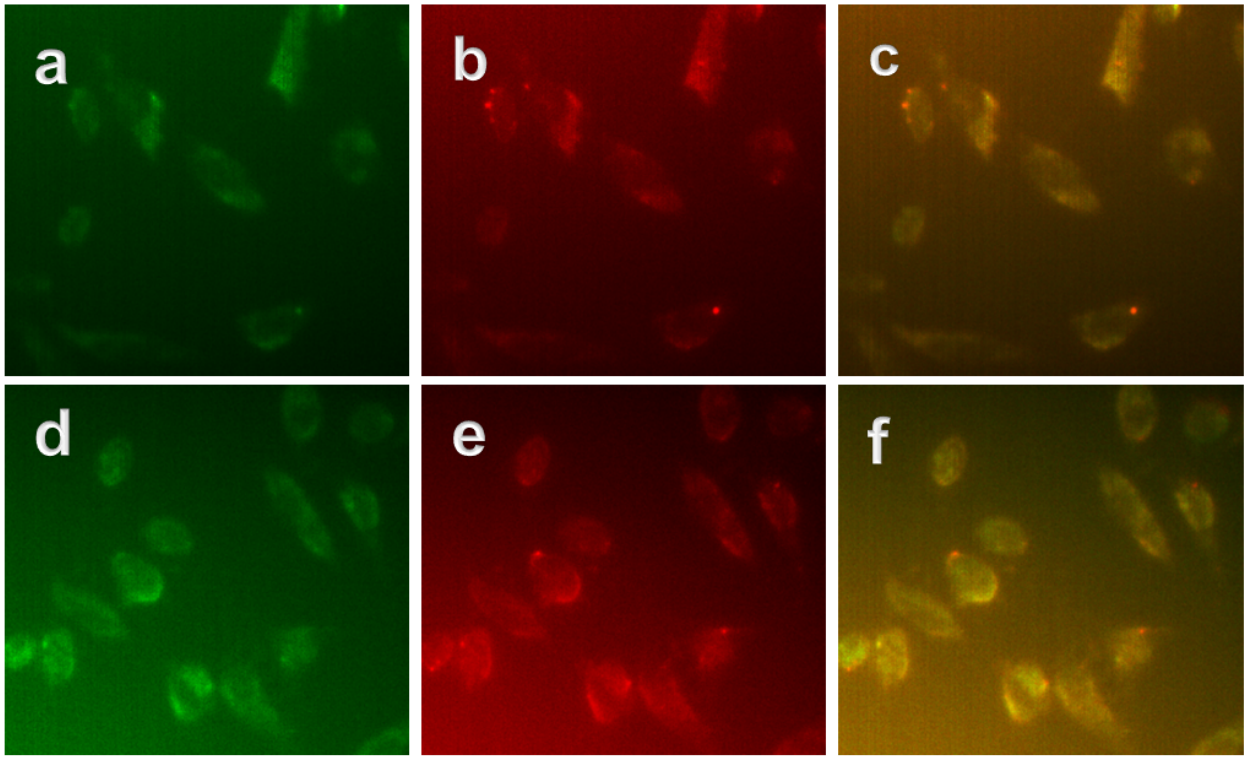

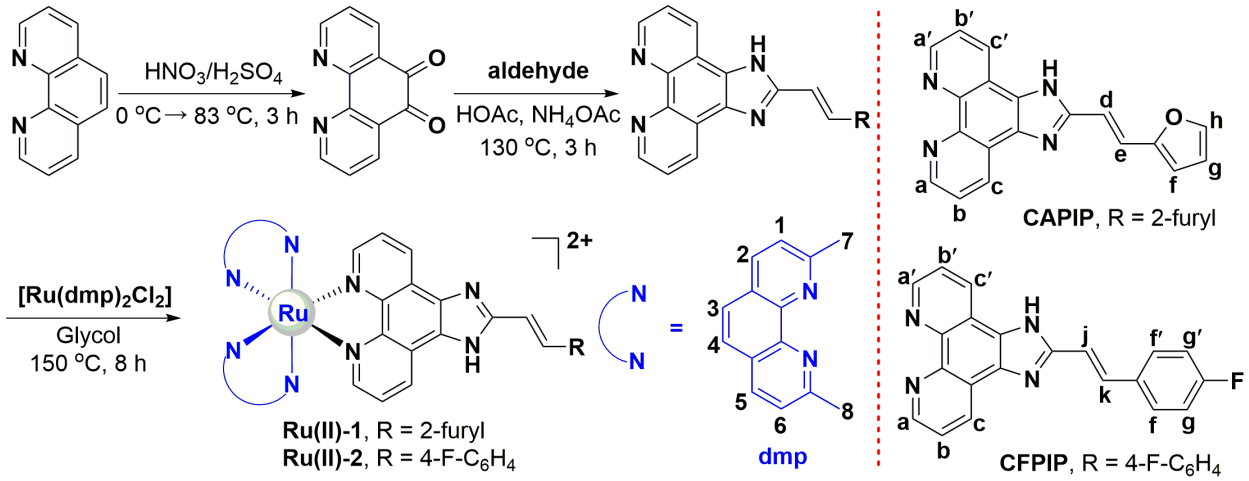

Research highlights

- Two new ruthenium(II) complexes were synthesized and characterized.
- DNA-binding behaviors of the Ru(II) complexes were investigated.
- The Ru(II) complexes displays high cytotoxic activity against A549 cells.
- The complexes can induce apoptosis and increase intracellular ROS levels.
- The mitochondrial membrane potential, cell cycle arrest and cell invasion were investigated.